NTNU
Norwegian University of
Science and Technology

Dynamic buckling of end anchored floating bridges

Ørjan Storheim
Ingvild Kristine Haug Østby

Master of Science in Civil and Environmental Engineering
Submission date: June 2018
Supervisor: Ole Andre Øiseth, KT

Norwegian University of Science and Technology
Department of Structural Engineering

Department of Structural Engineering
Faculty of Engineering Science and Technology
NTNU- Norwegian University of Science and Technology

ACCESSIBILITY

MASTER THESIS 2018

SUBJECT AREA:	DATE: June 11, 2018	NO. OF PAGES:
Structural dynamics		92

TITLE:

Dynamic buckling of end anchored floating bridges

Dynamisk knekking av endeforankrede flytebruer

BY:

Ingvild Kristine Haug Østby
Ørjan Storheim

SUMMARY:
The Bjørnafjord bridge is a floating bridge planned to be a part of The Norwegian Public Roads Administrations ferry-free road project along E39. This thesis looks into the dynamic behavior of this bridge, focusing of dynamic buckling.

This thesis looks into three simplified versions of the bridge, a 5000 meters long column with a lumped mass, an arch with horizontal length of 4600 meters and a very simplified bridge model. All three models have been tested for linear buckling, nonlinear buckling and dynamic buckling.

In regards to dynamic buckling, analyses show that all three models have unstable areas around the natural frequency, resonance, and double the natural frequency, parametric resonance. For the arch model and the simplified bridge, analyses were also run with a stochastic loading. The results from these analyses show that parametric excitation might also occur by a random load.

RESPONSIBLE TEACHER: Ole Andre Øiseth

SUPERVISOR(S): Aksel Fenerci, Øyvind Wiig Petersen

CARRIED OUT AT: NTNTU, Department of Structural Engineering

Summary

The Norwegian Public Roads Administration are currently working on a ferry-free road project along E39 on the western coast of Norway. As a part of this a bridge over Bjørnafjorden is planned. This bridge is a floating bridge with a cable stayed part. This thesis looks into the dynamic behaviour of this bridge, focusing on dynamic buckling.

Buckling is defined as a phenomenon where a mathematically perfect structure reaches an equilibrium state which is no longer stable when a critical force is applied. Dynamic buckling happens when the structure becomes unstable at certain load frequencies and load amplitudes. The loading may force the structure to get increasing deformations without an increase of load. Parametric resonance, or parametric excitation is also an important phenomenon regarding dynamic buckling. Parametric resonance occurs when two things oscillate together, the frequencies match, and one is unstable. Particularly when the load frequency is equal to double the natural frequency the structure will become unstable by parametric resonance.

A big part of this thesis is trying to establish which frequencies and load amplitudes that makes the bridge unstable. To establish these, three different models have been created, a simple column, a simple arch and a simplified bridge model. Each of these have been tested for the same kind of analyses, a linear buckling analysis, a nonlinear buckling analysis and a dynamic buckling analysis. In the dynamic analyses the loads are based on the critical linear buckling load P_{cr}. Since only the dynamic behaviour is of interest the applied loads are less than P_{cr}. All three models show the same response regarding the unstable areas. The first unstable area is detected around the natural frequency, this is expected as the structures will go into resonance when the load frequency is near the natural frequency. Next an area around double the natural frequency is an area with high deformations, all three models gets high deformations and experience parametric excitation. The unstable areas seem to be unstable for loads between $0.4P_{cr}$ and $0.7P_{cr}$, except for the arch model with a very high damping and parametric excitation does not occur until the loading is about $0.55P_{cr}$.

The next part of the thesis is trying to determine whether the arch model and the bridge model gets unstable by random loading. Several analyses were run with a load frequency in the area of parametric resonance, $\omega \approx 2\omega_n$. These analyses show that the external power is higher than the dissipated power when the models experience parametric resonance. The arch model did not have excess energy in a long enough amount of time to get into parametric resonance, the bridge model however experienced what could be seen as parametric resonance for the stochastic processes with the narrowest bandwidths. Both models did however get high displacements caused by a very high loading.

Samandrag

Styresmaktene i Noreg har planlagd ein ferjefri stamveg langs vestkysten av Noreg frå Kristiansand til Trondheim, dette prosjektet er ferjefri E39. I dette prosjektet er det planlagd ei bru over Bjørnafjorden. Brua er ei flytebru med eitt spenn støtta opp av brutårn. Denne oppgåva tar for seg den dynamiske oppførselen til brua, med hovudfokus på dynamisk knekking.

Knekking er definert som eit fenomen der ein matematsik perfekt struktur oppnår ein likevektstilstand som ikkje lenger er stabil når ei kritisk last vert påført. Dynamisk knekking inntreff når strukturen vert ustabil ved visse lastfrekvensar og lastamplituder. Lasta fører til at konstruksjonen får stadig aukande deformasjonar utan ei auke i påført last. Parametrisk resonans er eit viktig fenomen som kan opptre ved dynamisk knekking. Han oppstår når to gjenstandar oscillerer saman, der frekvensane er like og ein er ustabil. Konstruksjonen kan verte ustabil grunna parametrisk resonans særskild ved dobbel eigenfrekvens.

Ein stor del av denne oppgåva går ut på å etablere kva frekvensar og lastamplituder som gjer brua ustabil. For å etablere dette er det modellert tre ulike modellar, fyrst ei heilt enkel søyle, deretter ein enkel boge og til sist ein forenkla brumodell. Desse vart testa med same type analyser, ei lineær knekkanalyse, ei ikkje-lineær knekkanalyse og ei dynamisk knekkanalyse. I den dynamiske knekkanalyse er lastene som er påført basert på den lineære knekklasta P_{cr}, ettersom berre den dynamiske oppførselen er ønska er lastene som er nytta under P_{cr}. Alle dei tre modellane syner den same responsen i dei ustabile områda. Det første ustabile område oppstår rundt eigenfrekvensen, dette er venta ettersom konstruksjonen oppnår resonans når lastfrekvensen er nær eigenfrekvensen. Det neste området med store deformasjonar oppstår rundt den doble eigenfrekvensen. Alle dei tre modellane får store deformasjonar og er utsett for parametrisk resonans. Dei ustabile områda oppstår for laster mellom $0.4P_{cr}$ og $0.7P_{cr}$, med unntak av bogemodellen med høg demping der parametrisk resonans ikkje oppstår før lasta er rundt $0.55P_{cr}$.

Den neste delen av oppgåva tar for seg om bogemodellen og brumodellen vert ustabile når dei vert utsett for ei tilfeldig last. Fleire analyser vart kjørt med ein lastfrekvens i området rundt parametrisk resonans, $\omega \approx 2\omega_n$. Desse analysene syner at den ytre påførde energien er høgare enn det som vert dempa ut av konstruksjonen når parametrisk resonas oppstår. Bogen hadde ikkje tilstrekkeleg med energi over eit langt nok tidsrom til å oppnå parametrisk resonans. Brua oppnådde ein oppførsel som likna på parametrisk resonans for den stokastiske prosessen med den minste båndvidda. Både bogen og brua vart utsett for store deformasjonar grunna ei veldig høg last.

Preface

This thesis is written as a conclusion of our master's studies at the Department of Structural Engineering at NTNU. Here investigations on how a floating bridge responds to harmonic and stochastic loads have been made.

We would like to thank our supervisor associate professor Ole Øiseth for his guidance during this work, and also PhD Aksel Fenerci for his input and corrections during our process. Finally we would like to thank PhD Knut Andreas Kvåle for providing the simplified bridge model, and his help in the use of the model. We would also like to thank Bernardo da Costa at Statens Vegvesen for his help in dealing with problems related to the bridge itself.

Ingvild Kristine Haug Østby

Ørjan Storheim

Trondheim, June 11, 2018

Contents

Summary i

Samandrag iii

1 Introduction **1**

2 Theory **3**

2.1 Linear buckling 3

2.1.1 Equation of motion 4

2.1.2 Static buckling 5

2.1.3 A simple arch 7

2.2 Nonlinear buckling 10

2.2.1 Column 11

2.2.2 Arch 11

2.3 Dynamic buckling 14

2.3.1 Analytical expressions 14

2.3.2 Parametric resonance 16

2.3.3 Arch buckling types 19

2.4 Stochastic load and spectra 19

2.4.1 Spectra 23

2.4.2 Narrow and broad banded processes 24

2.5 Difference between static and dynamic buckling 26

2.6 Energy methods 27

3 FE-analysis 29

3.1 Column model 29

3.1.1 Geometry 30

3.1.2 Element type 31

3.1.3 Material properties 31

3.2 Arch model 32

3.2.1 Geometry 32

3.2.2 Element type 33

3.2.3 Material properties 33

3.3 Bridge model 34

3.3.1 Geometry and material properties 34

3.3.2 Element type 36

3.4 Column results 37

3.4.1 Euler buckling 37

3.4.2 Nonlinear buckling 38

3.4.3 Dynamic buckling 39

3.5 Arch results 44

3.5.1 Euler buckling 44

3.5.2 Nonlinear buckling 45
3.5.3 Dynamic buckling 47
3.6 Bridge results 54
3.6.1 Linear buckling 54
3.6.2 Nonlinear buckling 54
3.6.3 Dynamic buckling 55

4 Discussion **60**

5 Conclusion **65**

6 Further work **66**

Bibliography **67**

A Cut-off criterion for analysis **69**

B MATLAB-script **70**

C Challenges with the arch **75**

D Stochastic plots **77**

Chapter 1

Introduction

As a part of the ferry free road project on the western coast of Norway, from Kristiansand to Trondheim, it is planned a bridge over Bjørnafjorden. The Bjørnafjord bridge is south of Bergen, in Hordaland county, and it crosses a strait that is about 4600 meters across. The bridge itself is a floating bridge with a cable-stayed part. In modern engineering the approach is to create as slender structures as possible; this may, however, cause unwanted problems, specifically related to dynamic behaviour. One such problem is dynamic buckling, which is the main topic of this thesis. Dynamic buckling is caused by one or more dynamic loads. Such loads cause the system to oscillate and these oscillations may cause deformations so large that the system will reach failure. One particular effect caused by the dynamic loading is parametric resonance. That is when the applied load has a frequency that match m times the natural frequency. This may cause the system to have exceedingly large deformations.

The Bjørnafjord bridge will be about 4600 meters long, and the radius is around 5000 meters. The bridge is planned to have a curved geometry so the forces from waves and wind will be taken up in the end anchors as axial loads.

In this thesis dynamic buckling of an end anchored floating bridge is presented. Three different models have been constructed to investigate how dynamic buckling may affect the system. First a simple column with a point mass at the mid-point is presented, the column is 5000 meters long, and is a very simplified version of the bridge. Secondly an arch with distributed mass is presented, the arch has a horizontal length of 4600 meters,

and a radius of 5000 meters, one step closer to the actual bridge. Finally a simplified model of the real bridge is presented. In the simplified model, the cable-stayed part of the bridge is disregarded, and it is modelled just as a floating bridge.

All the models have been exposed to the same type of analyses, a linear buckling analysis, a non-linear buckling analysis and finally a dynamic buckling analysis. The arch model and the bridge model was in addition to a harmonic buckling analysis, exposed to a stochastic load in order to simulate the wave and wind loading for the real bridge.

Chapter 2

Theory

In this chapter the theory of buckling is described, and equations are developed which will be used in subsequent chapters. The buckling analysis is based on solving the equation of motion for the system, both in the static and the dynamic case. In the static case the equation of motion simplifies to the regular 4th order differential equation for the system.

2.1 Linear buckling

For the static case the problem can either be linear or nonlinear. In the first section the linear buckling case known as Euler buckling is presented, whereas nonlinear buckling is presented in the second section. The derivations of the equations in sections 2.1.1 and 2.1.2 follow Lindberg [1].

2.1.1 Equation of motion

To establish the equation of motion, we consider a simply supported uniform bar under compression, see figure 2.1a. below.

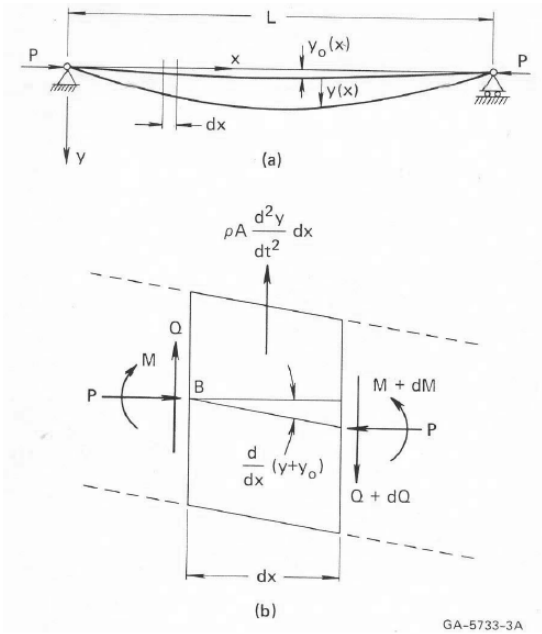

Figure 2.1: Bar nomenclature and element of length, Lindberg [1], page 10

By considering dynamic equilibrium and the moment-curvature relation for the bar, summation of forces in the y direction gives

$$-Q - \rho A \frac{\partial^2 y}{\partial t^2} dx + (Q + dQ) = 0,$$

and

$$M - \rho A \frac{\partial^2 y}{\partial t^2} dx \frac{dx}{2} + (Q - dQ)dx - (M + dM) + P \frac{\partial}{\partial x}(y + y_0)dx = 0.$$

By neglecting terms of second order, shear deformations and shortening of the bar in its longitudinal axis, the equation of motion for the simple system becomes

$$EI \frac{\partial^4 y}{\partial x^4} + P \frac{\partial^2}{\partial x^2}(y + y_0) + \rho A \frac{\partial^2 y}{\partial t^2} = 0. \tag{2.1}$$

2.1.2 Static buckling

Buckling is defined as a phenomenon where a mathematically perfect column reaches an equilibrium state which is no longer stable when a critical force, P_{cr}, is applied. Static buckling is based on the following assumptions:

- The column is straight and has no imperfections.
- The material is elastic and follows Hooke's law.
- The load is applied on an axis through the area centre of the cross section.
- Displacements in the column are small.

The critical force, P_{cr}, is found by equilibrium of the column in a displaced state.

For the static case, the inertia term in the general equation of motion, equation 2.1, is neglected, and it becomes

$$EI\frac{d^4y}{dx^4} + P\frac{d^2y}{dx^2} + P\frac{d^2y_0}{dx^2} = 0.$$

For a beam with no initial deflection, $y_0 = 0$, the solution of the equation above is

$$y = A\sin(kx) + B\cos(kx) + Cx + D, \tag{2.2}$$

and by imposing the boundary conditions for a simply supported beam, equation 2.2 has the nontrivial solution

$$\sin(kL) = 0$$

which gives

$$kL = \pm n\pi,$$

where n is an integer. Inserting $k^2 = P/EI$ gives

$$P_n = \frac{\pi^2 EI}{L^2} n^2. \tag{2.3}$$

If the beam has initial deflection $y_0(x)$, then the solution will be on the form

$$y_0(x) = \sum_{n=1}^{\infty} a_n \sin\left(\frac{n\pi x}{L}\right) \tag{2.4}$$

where the coefficients a_n are given by

$$a_n = \frac{2}{L} \int_0^L y_0(x) \sin\left(\frac{n\pi x}{L}\right) dx.$$

Inserting the solution from equation 2.4 into the equation of motion 2.1, and setting $k^2 = P/EI$, gives the differential equation for the imperfect bar

$$\frac{d^4 y}{dx^4} + k^2 \frac{d^2 y}{dx^2} = k^2 \frac{n^2 \pi^2}{L^2} \sin\left(\frac{n\pi x}{L}\right) \tag{2.5}$$

Equation 2.5 has a particular solution on the form

$$y_p = \sum_{n=1}^{\infty} A_n \sin\left(\frac{n\pi x}{L}\right),$$

and by inserting this into equation 2.5 the coefficients A_n are established

$$A_n = -\frac{P a_n}{P - P_n}.$$

The complete solution is then

$$y(x) = A\sin(kx) + B\cos(kx) + Cx + D - \sum_{n=1}^{\infty} \frac{P a_n}{P - P_n} \sin\left(\frac{n\pi x}{L}\right).$$

By applying the boundary conditions, and that the load P is arbitrary, the general solution becomes

$$y(x) = -\sum_{n=1}^{\infty} \frac{Pa_n}{P - P_n} \sin\left(\frac{n\pi x}{L}\right)$$

As P approaches the critical load given by equation 2.3 the deflections become arbitrarily large. The motion is unstable for any load greater than the lowest critical load, that is, for $n = 1$. In the area around P_1, the lowest critical load, the first term of the summation above dominates. Hence, the critical load for the system is

$$P_{cr} = \frac{\pi^2 EI}{L^2}. \tag{2.6}$$

2.1.3 A simple arch

An arch with fixed ends, and a radially applied distributed load, will generally buckle in one of two shapes as illustrated in figure 2.2 below.

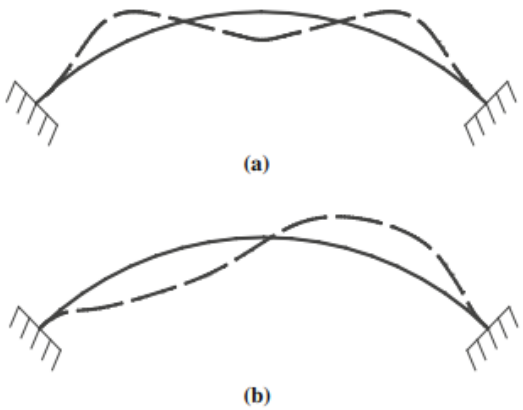

Figure 2.2: Symmetric buckling mode **(a)** and bifurcation buckling **(b)**, J.Zhu et al. [2], page 1843

The arch will buckle symmetrically if it has no imperfections and asymmetrically if it has imperfections. Since the asymmetric mode requires the least amount of energy to be excited, it is the one that will occur in regular arches. A perfect arch is after all just a theoretical concept.

The expressions in this section follow Karnovsky [3]. Behaviour of a uniform circular arch of radius R and flexural rigidity EI may be described by the second order differential equation, known as Boussinesq's equation, below

$$\frac{d^2v}{d\phi} + v = -\frac{MR^2}{EI} \tag{2.7}$$

where v is a displacement point of the arch in the radial direction, ϕ is the angle measured from the central angle to the point v and M is the bending moment which is produced when the arch becomes unstable.

For a fixed arch, equation 2.7 becomes

$$\frac{d^2v}{d\phi^2} + n^2v = -\frac{M_0R^2}{EI\sin(\alpha)}$$

due to the moment M_0 at each end caused by the loading, α is the central angle of the arch. The total solution of the equation above is

$$v = A\cos(n\phi) + B\sin(n\phi) + \frac{1}{n^2-1}\frac{M_0R^2}{EI\sin(\alpha)}\sin(\phi)$$

For a point on the arch on the axis of symmetry, the radial displacement is $v = 0$, and the equations for radial displacement and slope are

$$v = B\sin(n\phi) + \frac{C}{n^2-1}\sin(\phi)$$
$$\frac{dv}{d\phi} = Bn\cos(n\phi) + \frac{C}{n^2-1}\cos(\phi)$$

Imposing the boundary conditions, no displacement or rotation at each end, gives

$$B\sin(n\alpha) + \frac{C}{n^2-1}\sin(\alpha) = 0$$
$$Bn\cos(n\alpha) + \frac{C}{n^2-1}\cos(\alpha) = 0$$

These equations are algebraic and homogeneous, hence the nontrivial solutions are possible if the determinant of the matrix consisting of coefficients of the unknowns is equal to zero. Simplifications give the equation of critical loads

$$\begin{vmatrix} \sin(n\alpha) & \frac{1}{n^2-1}\sin(\alpha) \\ n\cos(n\alpha) & \frac{1}{n^2-1}\cos(\alpha) \end{vmatrix} = 0,$$

or written in another way

$$\frac{\alpha}{\tan(\alpha)} = \frac{n\alpha}{\tan(n\alpha)} \tag{2.8}$$

Equation 2.8 has the minimum roots as shown in table 2.1 below.

α	30°	45°	60°	90°
n	8.621	5.782	4.375	3.000

Table 2.1: Minimum root of transcendental equation

The analytic solution requires solving transcendental equations, hence approximations are required. Using

$$q_{cr} = (n^2 - 1)\frac{EI}{R^3} \tag{2.9}$$

where n is approximated based on the minimum root of the transcendental equation 2.8 above.

2.2 Nonlinear buckling

If a slender structure is exposed to a compressive loading, it may get a dramatic reduction of structural stiffness; this leads the structure to become unstable. Buckling can be referred to as a situation where a very small increase in load, causes a very large displacement. This is caused by the axial strain energy that is converted into bending strain energy, without change in the external load. In slender columns, the axial stiffness is a lot higher than the bending stiffness, so large bending deformations will occur if axial strain energy is converted into bending strain energy. The stiffness consists of two components, the elastic stiffness, $[K_M]$ and the geometric stiffness, $[K_G]$. The elastic stiffness is dependent on the material properties of the structure, and the geometric stiffness depends on the structures state of stress. With tensile stresses the stiffness will increase, and with compressive stresses the structure will get a reduction of its stiffness.

$$[K_T] = [K_M] + [K_G] = [0]$$

Buckling occurs when the total stiffness of the structure becomes singular, and may be expressed as a eigenvalue problem:

$$([K_M] + \lambda[K_G])\{\phi\} = [0]$$

Where λ represents the eigenvalue and φ the corresponding eigenvector that represents the buckling shape. Thus the buckling load can be found with the following equation:

$$P_{CR} = \lambda P$$

From the lecture in Nonlinear FEM fall 2017 [4].

2.2.1 Column

The linear buckling analysis is based on a theoretical column without imperfections, and usually involves very little deformation prior to buckling. But a real column however, will always have some imperfections. Either in regard to where the load is placed, or in the geometry of the beam. This results in a lower critical load than what the linear buckling analysis gives, and the column will buckle before it reaches the analytic value. A nonlinear buckling analysis will take into account that the load and the geometry will change when the structure is deformed.

A nonlinear buckling analysis can be performed by using the "Static Riks method". This method is used to predict unstable, geometrically nonlinear collapse by using an iterative calculation of the structures stability. The Static Riks method uses both the deformation and the load magnitude as unknowns, and solves for the two simultaneously. This method uses fixed increments along the static equilibrium path, and the load value may increase or decrease with the solution [5]. To include the non-linearities a stiffness matrix is formed, which includes the effect of the changing geometry. The method will give the columns equilibrium path, where buckling can be defined as the point where the tangent stiffness is equal to zero. The tangent stiffness can only be equal to zero if there are no imperfections present, which is only a theoretical case.

2.2.2 Arch

The in-plane behaviour of a shallow arch will become nonlinear as the external loading increases. At a certain value the arch will buckle in bifurcation mode an asymmetric buckling shape, or in a snap-through mode. Snap-through buckling may also be referred to as symmetric buckling.The deformation before the arch buckles is significant and nonlinear, and the effects of that will therefore have to be included in the buckling analysis. A linear approach to a buckling analysis of an arch will be non-conservative, and estimate a higher critical load. A nonlinear buckling analysis will give the whole equilibrium path for an arch, and will therefore give more valuable information and give a better estimate on the critical buckling load [2].

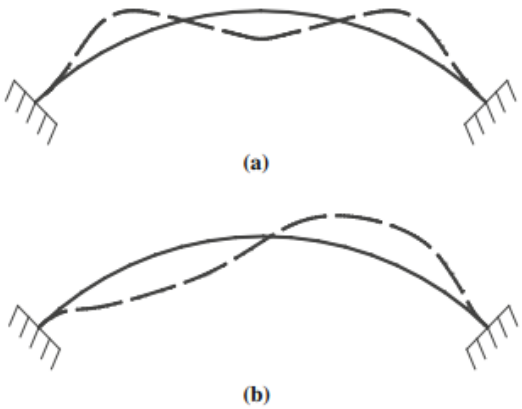

Figure 2.3: Symmetric buckling mode **(a)** and bifurcation buckling **(b)**, J.Zhu et al. page 1843 [2]

An arch without imperfections and with perfect circular geometry will only deform symmetrically when a radial load is applied. An arch with imperfections, however, may buckle non-symmetrically; which is also called bifurcation buckling. The buckling modes also depend on the loading conditions. Figure 2.3 shows two of the typical buckling modes for an arch, figure 2.3 **a** shows the symmetric buckling mode, and figure 2.3 **b** shows the bifurcation buckling mode. [2]

Figure 2.4 below shows a typical equilibrium path for nonlinear buckling of a circular arch. Both the symmetrical and non-symmetrical paths are the same before buckling occurs. After the first bifurcation point, the bifurcation path will fall almost linearly until the next bifurcation point. After that the paths will again follow the same curve. [2]

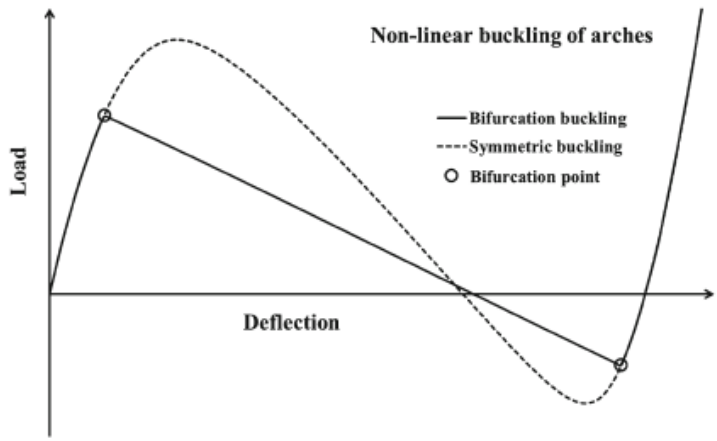

Figure 2.4: Nonlinear buckling arch, J.Zhu et al. page 1844 [2]

Several approaches are adopted to solve the nonlinear buckling problem for arches analytically. The problem may be solved by using the principle of stationary potential energy with nonlinear strain, where the critical condition is defined by Pi et al. [6] as when the second variation of the total potential is equal to zero [6]. The nonlinear buckling problem may also be solved by finite element analysis, and the Static Riks method. The Riks method works well with snap-through problems, and post-buckling analysis where imperfections are implemented for an accurate analysis. As mentioned in the earlier section, the Riks method iteratively calculates the deformation and load simultaneously, and follows the equilibrium path beyond limit points. This makes it possible to follow the post-buckle equilibrium path. [5]

2.3 Dynamic buckling

Static buckling concerns the steady load that can be safely carried by the column; however, if the load is varying with time, the problem becomes dynamic. One such instance is if the load is suddenly applied and removed; then the maximum load that the column can sustain may be far greater than in the static case. For such a case, the main concern is to specify the load and then seek the response of the system. Dynamic buckling may also be caused by stochastic loads such as, for instance, wind or waves.

To perform a dynamic analysis, two different ways are commonly applied. The analysis may be deterministic, in which case the complete load time history has to be known, or stochastic, where the loads are specified using statistical concepts.

Dynamic buckling of systems may become quite complicated to solve and analytical expressions are only available for relatively simple systems. In the following sections, analytical expressions for a simply supported beam with an axial load $P(t)$ and initial displacement y_0 are developed.

The analytical expressions developed below, section 2.3.1, follow Lindberg [1], and the loading applied in this case is a load which is suddenly applied and then removed.

2.3.1 Analytical expressions

For a simply supported beam with an axial load P on top of the column and initial displacement y_0; the equation of motion is

$$EI\frac{\partial^4 y}{\partial x^4} + P\frac{\partial^2}{\partial x^2}(y + y_0) + \rho A\frac{\partial^2 y}{\partial t^2} = 0$$

The column is simply supported, hence both the deflection and bending moments are zero at both ends. The boundary conditions for the system then becomes

$$y = \frac{d^2 y}{dx^2} \qquad \text{at } x = 0 \text{ and } x = L$$

By imposing these boundary conditions, the solution of the equation of motion above may be expressed in the form

$$y(x,t) = \sum_{n=1}^{\infty} q_n(t) \sin\left(\frac{n\pi x}{L}\right)$$

If the bar has initial displacement y_0, this displacement may also be expressed as a Fourier series,

$$y_0(x) = \sum_{n=1}^{\infty} A_n \sin\left(\frac{n\pi x}{L}\right)$$

where the coefficients are found with

$$A_n = \frac{2}{L}\int_0^L y_0(x) \sin\left(\frac{n\pi x}{L}\right).$$

Introducing dimensionless variables

$$w = \frac{y}{r}, \qquad \xi = kx = \frac{sx}{r}, \qquad \tau = \frac{s^2 ct}{r},$$

where r is the radius of gyration for the cross section, c is the wave speed of axial stress waves in the bar and s is the ratio of the lateral deflections with respect to the radius of gyration. Using the assumption that the bar is initially at rest, the final solution of the equation of motion is

$$w(\xi, r) = \begin{cases} \sum\limits_{n=1}^{\infty} \frac{a_n}{1-\eta^2} \left(\cosh(p_n\tau) - 1\right) \sin\left(\frac{n\pi\xi}{l}\right) & \text{if } \eta < 1, \\ \sum\limits_{n=1}^{\infty} \frac{a_n}{1-\eta^2} \left(\cos(p_n\tau) - 1\right) \sin\left(\frac{n\pi\xi}{l}\right) & \text{if } \eta > 1, \end{cases}$$

where $\eta = \frac{n\pi}{l}$ is the wave number.

2.3.2 Parametric resonance

Parametric resonance is a phenomenon not caused by external excitation, but by time-varying changes in the parameters [7]. If a structure gets unstable under static loading, parametric resonance may occur under harmonic loading. A column exposed to periodic dynamic loading will vibrate in the axial direction. At certain combinations of the frequency ratio and the amplitude of the dynamic load, the axial vibrations of the column may switch to lateral vibrations with increasing amplitude, leading to lateral parametric resonance instability [8].

Simply put, if two things are oscillating together, and the frequencies match and one is unstable, parametric resonance can occur. For instance, for a column under harmonic loading, the column will start to vibrate if the loading has a frequency of $m\omega_n$, where ω_n is the natural frequency of the column and m is a positive integer, the system may become unstable due to parametric resonance.

A column exposed to axial harmonic loading, $P(t) = P_0 \cos(\omega t)$, with a lateral deflection u at the mid-point, a lumped mass m at the middle of the beam and damping parameter c will have the following equation of lateral vibration:

$$\frac{\partial^2}{\partial x^2}\left(EI\frac{\partial^2 u}{\partial x^2}\right) + \frac{\partial}{\partial x}\left(P(x,t)\frac{\partial u}{\partial x}\right) + m\frac{\partial^2 u}{\partial t^2} + c\frac{\partial u}{\partial t} = 0 \tag{2.10}$$

According to Huang et. al [8] this equation can be rewritten into equation 2.16 by the following steps:

The displacement $u(x,t)$ is the superposition of the modal shapes of the column:

$$u(x,t) = \sum_{n=1}^{\infty} y_n(t) \sin\frac{n\pi x}{L} = 0 \tag{2.11}$$

Here $y_n(t)$ is the n-th modal response of the column. Substituting equation 2.11 into equation 2.10 gives the following equation:

$$\sum_{n=1}^{\infty}\left[EI\frac{n^4\pi^4 y_n(t)}{L^4} - p(t)\frac{n^2\pi^2 y_n(t)}{L^2} + m\ddot{y}_n(t) + c\dot{y}_n(t)\right]\sin\frac{n\pi x}{L} = 0 \quad (2.12)$$

In equation 2.12 $\sin(\frac{n\pi x}{L})$ does not vanish for all $x \in [0, L]$, so the first part of the equation must be equal to zero:

$$EI\frac{n^4\pi^4 y_n(t)}{L^4} - p(t)\frac{n^2\pi^2 y_n(t)}{L^2} + m\ddot{y}_n(t) + c\dot{y}_n = 0 \quad (n = 1, 2, ..., \infty) \quad (2.13)$$

Equation 2.13 can be rewritten into:

$$\omega_n^2\left[1 - \frac{p(t)}{P_{cr}}\right]y_n(t) + \ddot{y}_n(t) + \frac{c}{m}\dot{y}_n(t) = 0 \qquad (n = 1, 2, ..., \infty) \qquad (2.14)$$

Here ω_n is the n-th natural frequency, and P_{cr} is the n-th Euler buckling load of the column under static uniform loading.

The periodic loading $P(t)$ with time-period T can be expressed as a Fourier series:

$$p(t) = P_0 + \sum_{k=1}^{\infty} p_k \cos(k\theta t) \qquad (2.15)$$

In this equation P_0 is the static component of $p(t)$ and p_k is the amplitude of the k-th harmonic wave component, and θ is the circular frequency of the loading with $\theta = \frac{2\pi}{T}$. Combining equation 2.14 and 2.15 leads to equation 2.16:

$$\ddot{y}_n(t) + \frac{c}{m}\dot{y}_n + w_n^2[1 - 2\mu\cos(\omega t)]y_n = 0 \qquad (2.16)$$

Equation 2.16 above is called Mathieu's equation. It is a linear differential equation with variable coefficients. Here μ is the parameter of the excitation amplitude, given by:

$$\mu = \frac{P}{2(P_{cr} - P_0)}$$

The main concern with Mathieu's equation is whether the solution is bounded for the given values of ω, μ and $\frac{c}{m}$. If all solutions to the equation are bounded, then the corresponding point in the P - ω parameter plane is stable. However if there exists a solution that is unbounded, the point is unstable.

Solving Mathieu's equation, gives the following Beliaev's formula [8]:

$$\frac{\omega}{2\omega_n} = 1 \pm \frac{\mu}{2}$$

Solution to this problem for a slender column results in the graph below, figure 2.5, showing the μ - $\frac{\omega}{2\omega_n}$ plot for the first instability region.

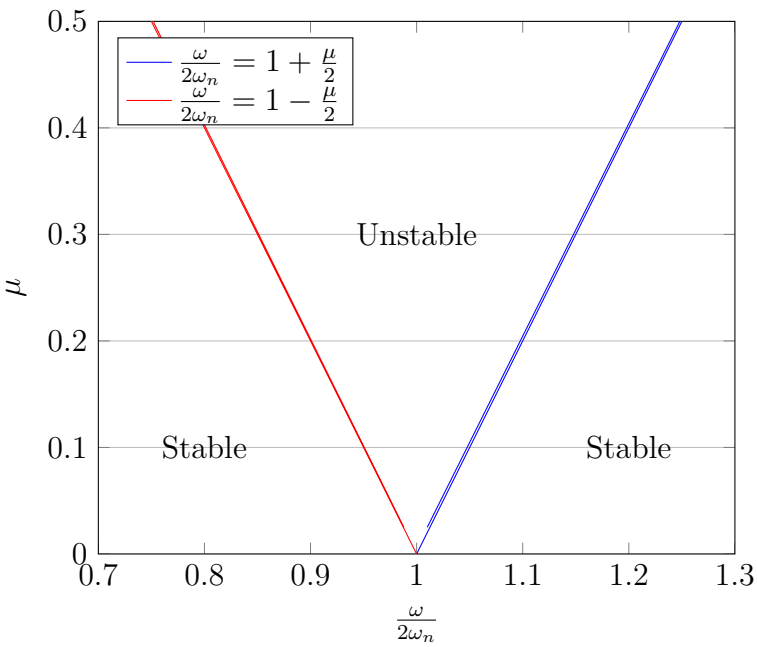

Figure 2.5: First instability region

2.3.3 Arch buckling types

Buckling of a column or an arch is a stability problem; when buckling occurs the system becomes unstable. According to Kounadis and Raftoyiannis [9], dynamic buckling of an arch is defined as the state for which an escaped motion becomes either unbounded or of very large amplitude. The minimum load corresponding to this situation is defined as the dynamic buckling load.

For an arch, the two main buckling cases are snap-buckling and bifurcation type buckling. Snap-buckling means that the structure suddenly jumps from one stable equilibrium configuration to another one, while bifurcation type buckling means that the structure deforms along a secondary path representing an asymmetric mode after it has exceeded a certain load level. Arches subjected to symmetric vibration loads, will have symmetric forced vibrations in the frequency of the loads. When the perturbation frequencies match the natural frequencies, resonance will take place. Parametric resonance will occur as well, if the vibrations have double the natural frequency [10].

2.4 Stochastic load and spectra

The previous sections regarding dynamic buckling have focused on a harmonic or deterministic loading. Another part of dynamic loading is the stochastic loading, or random loading. Nature loads such as wind or waves are examples of the phenomenon stochastic processes.

A stochastic process is a set of stochastic variables which is dependent on at least one continuous or discrete parameter. This parameter can be time t, and the process can then be describes as $X(t, a)$. The parameter a describes the process' random nature, $a \in A$ where A is the amount of possible outcomes, and t is the time. For a given $a = a_i$ the function $X(t, a)$ will be a deterministic function of t, and is denoted as one realisation of the stochastic process. [11]

For the case of stochastic processes caused by nature, the process will be a continuous process where the sample space A is infinite. Natural processes are considered to have been running, and will continue running, over a long time period. For a construction exposed to random vibrations from

a stochastic process, the process is describes as a continuous stochastic process.

The theory of stochastic processes are based on statistics. By collecting data from many samples of the stochastic process, getting an ensemble average, it is possible to estimate the characteristic probability distribution [12].

Probability distribution

Probability distribution functions are used to describe a random process. At a specified time instance t, a first-order probability distribution of $X(t)$ is defined as:

$$F_1(x,t) = P\{X(t) < x\}$$

The second-order probability distribution considers two time instances t_1 and t_2. The probability of $X(t_1) < x_1$ and $X(t_2) < x_2$, the second-order probability distribution can be defined this way:

$$F_2(x_1,t_1;x_2,t_2) = P\{X(t_1) < x_1, X(t_2) < x_2\}$$

According to Newland [13], the probability distribution function gives the probability of a value of the random variable is less than x. To completely define the random process the distribution functions of all orders must be known. It is usually both unnecessary and difficult to define the probability functions of all orders. However, for many cases the first and second-order probability distribution functions are sufficient. Specially for a Gaussian random process, it is often sufficient with the first and second-order of the probability distribution function [12]. As the stochastic processes of nature usually has this Gaussian distribution these processes may be determined by the first and second-order of the process.

The stochastic process may be described as a stationary process. This means that the probability distribution functions of the ensemble are independent of the absolute time.

$$F_n(x_1,t_1;x_2,t_2;....;x_n,t_n) = F_n(x_1,t_1+\tau;x_2,t_2+\tau;....;x_n,t_n+\tau)$$

A stochastic process may be expected to be stationary when the physical factors influencing the system does not change over time [12]. The process may be weakly stationary or strictly stationary. A strictly stationary process is given as an example in the equation above where all probability distributions are independent of absolute time. A weakly stationary process is a process where only the first and second order probability distributions are independent of absolute time. If a process is stationary by first and second order it implies that all averages are independent of absolute time, the mean, the mean square, variance and standard deviation are independent of absolute time [13].

A stochastic process may also be homogeneous, this is when the process has equal probability distribution in all points, this means that the transition probability between two points only depend on the difference. [13]

Normally in the field of structural dynamics the process is assumed to be homogeneous and stationary.

Correlation

Correlation of a process is how two variables correspond with each other. In the field of stochastic processes the autocorrelation function and the cross-correlation function are two central concepts. The autocorrelation function for a random process $x(t)$ is defined by Newland [13] as the average value of the product $x(t)x(t+\tau)$. The prefix auto- signifies that the two random variables which are considered belong to the same random process. For a process that is sampled at time t, and again at $t + \tau$, the average value of the ensemble $E[x(t)x(t + \tau)]$ is the autocorrelation function for $x(t)$ if the process is stationary [13].

$$E[x(t)x(t + \tau)] = R_{xx}(\tau)$$

This shows how a process is correlated with itself at time t and at time $t + \tau$. To decide the degree of correlation between two different stationary processes $x(t)$ and $y(t)$ the cross-correlation function is used. The cross-correlation function is defined as:

$$R_{xy}(\tau) = E[x(t)y(t + \tau)]$$
$$R_{yx}(\tau) = E[y(t)x(t + \tau)]$$

The time history of a random process will not be periodic, and cannot be described by a discrete Fourier series. The process of a stationary random process $x(t)$ will also go on forever, so that the classical theory of Fourier analysis cannot be applied to a sample function. By analysing the autocorrelation function instead of the sample functions this can be overcome as the autocorrelation function gives information about the frequencies present in the stochastic process indirectly [13].

Spectral density

The auto-spectral density gives information about where the average power is distributed as a function of frequency. The auto-spectral density is found from the Fourier transform of the autocorrelation function for a stationary process where the mean values is equal to zero:

$$S_{xx}(\omega) = \int_{-\infty}^{\infty} R_{xx}(\tau) e^{-i\omega\tau} d\tau$$

And the autocorrelation function is found from the reverse Fourier transform of the auto-spectral density function:

$$R_{xx}(\tau) = \int_{-\infty}^{\infty} S_{xx}(\omega) e^{i\omega\tau} d\omega$$

If $\tau = 0$ the most important property of the spectral density becomes apparent:

$$R_x(\tau = 0) = \int_{-\infty}^{\infty} S_x(\omega) d\omega = E[x^2]$$

This enables us to find the mean square value of a random stationary process. The relationship between the auto-spectral density of the load and the response can be found from the following equation:

$$S_{yy}(\omega) = |H(\omega)|^2 S_{xx}(\omega)$$

Where $H(\omega)$ is the frequency response function, known as equation 2.17 for a 1-DOF-system.

$$H(\omega) = (-\omega^2 m + i\omega c + k)^{-1} \tag{2.17}$$

The cross-spectral density can be found from the cross-correlation function:

$$S_{xy}(\omega) = \int_{-\infty}^{\infty} R_{xy}(\tau) e^{-i\omega\tau} d\tau$$

The cross-spectral density gives information about how the average power is distributed as function of frequencies in both $x(t)$ and $y(t)$. The cross-spectral density has the unit $(x \cdot y)/\omega$ [13].

2.4.1 Spectra

A spectrum is a relationship represented by a plot of the magnitude or relative value of some parameter against frequency. The power spectral density (PSD) functions describes how the energy of the signal is distributed as a function of frequency. Any signal that can be represented as a variable that varies with time has a corresponding frequency spectrum.

The load spectrum of a structure should give information about the load-time history, which is the variation of the load as a function of time.

In order to calculate the load from sea waves, a wave spectrum is a useful approach. Such a spectrum is based on measurements of the wave height over a time period. By sampling at an interval a time series can be created. Taking a fast Fourier transform of the time series and calculating the periodogram, a spectrum is created. Repeating this process several times and averaging the spectra, a final average spectrum is created.

2.4.2 Narrow and broad banded processes

Processes may generally be either narrow banded or broad banded, with white-noise as the limit of broad banded. A process is called narrow banded if the spectral density occupies only a narrow band of frequencies. A narrow banded stochastic process may be considered as a physical realisation of a harmonic process, and it is characterised by the following features:

- The realisations appear as harmonic functions dominated by an angular frequency ω_0, but with a slowly varying amplitude. Each zero upcrossing of the time axis is followed by a single local maximum.
- The auto-covariance function appears as a cosine function with slowly decreasing amplitude, providing a finite correlation length τ_0.
- The double auto-spectral density function appears with marked peaks in the vicinity of the angular frequency $\omega = \pm\omega_0$.

A narrow banded process is also characterised by $\tau_0 \ll T_0$ where $T_0 = \frac{2\pi}{\omega_0}$ represents the average period between zero upcrossings of the time axis. Narrow banded process may be found as, for instance, damping response processes for lightly damped structures under broad banded excitations.

According to Newland [13] a broad band process is one whose spectral density covers a broad band of frequencies and the time history is then made up of the superposition of the whole band of frequencies. In the limit when the frequency band extends from $\omega_1 = 0$ to $\omega_2 = \infty$, the spectrum is called white. A broad banded process is characterised by the following features:

- Realisations are irregular without a dominating frequency. Each zero up-crossing of the time axis may be followed by more than one local maximum.
- The auto-covariance function is vanishing for time separations larger than the average period between zero up-crossings $T_0 = \frac{2\pi}{\omega_0}$.
- The auto-spectral density function does not display any marked peak, not even at the mean angular up-crossing frequency ω_0.

The correlation length τ_0 for a broad banded process is of the length of the average zero up-crossing period, $\tau_0 \simeq T_0$. Broad banded processes may be found, for instance, as dynamic response processes for strongly damped structures.

An a-upcrossing means that the level $x = a$ is exceeded with positive slope, hence a zero up-crossing crosses at $x = 0$, examples of which are the points where the curve crosses the time axis in the top figure in figure 2.6a.

The auto-covariance function describes the strength of the linear relationship between the random variables x_i and x_{i+1}.

The realisation of a stochastic variable X is the value for a certain element $\omega_i \in \Omega$ in the sample space

$$x_i = X(\omega_i) \qquad \text{for } \omega_i \in \Omega$$

Figures 2.6a and 2.6b show examples of a time series and spectral density for a broad banded and narrow banded process respectively.

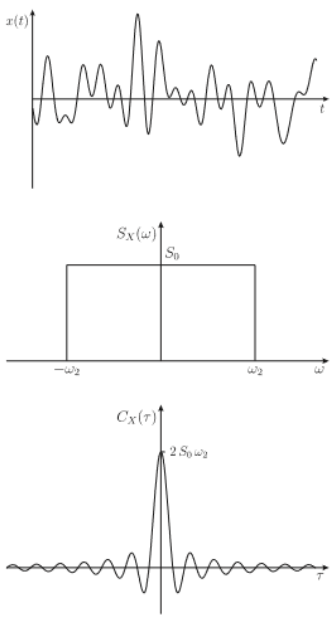

(a) Broad banded process, Naess [14], page 171

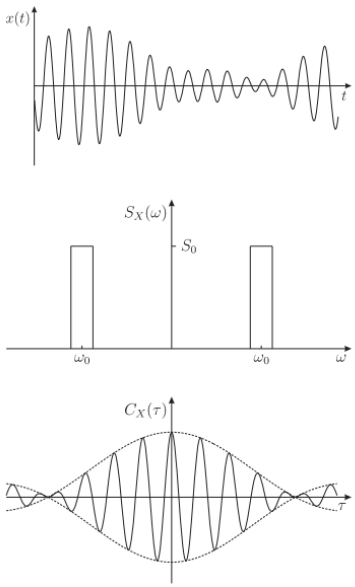

(b) Narrow banded process, Naess [14], page 172

Figure 2.6: Broad and narrow banded processes

If the energy is concentrated in a narrow band the load-time history will be similar to an amplitude modulated signal. One way to differentiate between narrow banded and broad banded is, according to Schijve [15], to use the irregularity factor k, which is defined as

$$k = \frac{\text{number of peak values}}{\text{number of level crossings of the reference level}}$$

If the spectrum is narrow banded, k $\approx$ 1, if it is broad banded generally k $>$ 1. The more irregular the spectrum, the larger value for k.

Also, if a spectrum is narrow banded a realisation of the process will behave like a sum of harmonic components with almost the same frequency. This can be seen in figure 2.6b where the envelope curve around the realisation x(t) is a harmonic function.

2.5 Difference between static and dynamic buckling

As mentioned in section 2.3.3, buckling is a stability problem. In static analysis the problem concerns finding the critical load which will result in an unbounded deflection if the system is given a disturbance. For the dynamic case, however, the disturbance has to be specified as initial conditions. According to Singer [16], in a perfectly straight and symmetric column, where the lateral initial conditions are all zero, a dynamic loading cannot initiate an unbounded lateral motion.

The main difference between static and dynamic buckling is that for static buckling one seeks the loading which, for the given initial conditions, causes unbounded deflection; while for dynamic buckling, the load is prescribed and one seeks the response. Also, for static linear buckling the buckling criteria are well defined, whereas for dynamic buckling these criteria have to be defined based on the problem at hand.

For a long column subjected to a suddenly applied axial load, it can withstand a load many times greater than the static Euler load. Under intense short-duration loading a very high-order deformation mode is experienced at buckling. In static buckling analysis the buckling mode is known and the maximum safe load is determined; in pulse buckling the load amplitude is prescribed and dictates the buckling modes, thus determining the maximum safe duration of its application.

Dynamic buckling may also be caused by parametric resonance. For a dynamic load it may happen that an integer multiple of the natural frequencies of the system are excited, causing the system to become unstable.

2.6 Energy methods

Using the energy of the system, the determination of the stability may be condensed to it most basic form as whether the energy which is contributed to the system is equal to the internal energy or not. In a vibrating structure, nonlinear restoring forces will dissipate a large amount of energy. If this amount of energy is equal to the energy imported into the system from external forces, the structure will be dynamically stable.

The system is dynamically stable if the external forces are in equilibrium with the internal reaction forces of the system, that is, if:

$$\boldsymbol{F}_{\text{ext}}(t) = \boldsymbol{F}_{\text{int}}(t),$$

where

$$\boldsymbol{F}_{\text{ext}}(t) = \boldsymbol{F}(t) - (\boldsymbol{M}\ddot{\boldsymbol{v}}(t) + \boldsymbol{C}\dot{\boldsymbol{v}}(t))$$

The energy of the internal and external forces is governed by the work done. The work done by the external forces is given by

$$W_{\text{ext}}(t) = [\boldsymbol{F}(t) - (\boldsymbol{M}\ddot{\boldsymbol{v}}(t) + \boldsymbol{C}\dot{\boldsymbol{v}}(t))]^T \boldsymbol{v}(t),$$

and the work done by the internal reactions is given by

$$W_{\text{int}} = \int_0^{\boldsymbol{v}} \boldsymbol{f}(\boldsymbol{v}, t) d\boldsymbol{v}$$

The total work done by the system is then

$$W(t) = W_{\text{ext}}(t) - W_{\text{int}}(t),$$

According to Xu and Li [17] the system becomes unstable if the imported energy to the structure is less than the work done W, if the amount of heat supplied to the system is neglected. If the system is able to damp the external forces then there is no excess energy in the system which can cause instabilities.

Chapter 3

FE-analysis

In this chapter the different Abaqus models and the results from the analyses are presented. For the static and harmonic loading the response of the structure is considered using the displacements, wheras for the stochastic load an energy consideration is performed, based on section 2.6. It also contains descriptions of the properties on which the different models are based.

3.1 Column model

The FEA software Abaqus is used to run the different analyses. For the first part of the assignment a slender simply supported column was modelled in Abaqus to simulate the bridge. In order to perform nonlinear analysis, geometric imperfections have been introduced in the model. These imperfections are based on the mode shapes from linear buckling analysis, this is a conservative approach, as the real imperfections will never be larger than the implemented imperfections.

3.1.1 Geometry

The column has the following parameters for the cross-section:

Height	3 m
Width	30 m
Thickness	0.04 m

Table 3.1: Geometric parameters

The length of the column is 5000 meters, with a rolled pin at one end and a fixed pin at the other, as illustrated in figure 3.1. Along the columns weak axis a boundary condition is set at each node to make sure the column will buckle in the correct direction. The column is also constrained from rotating along its own axis.

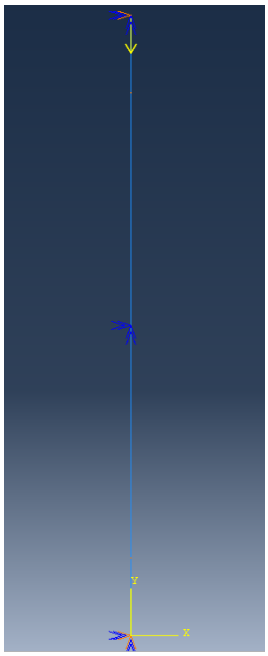

Figure 3.1: Abaqus model of the column

The natural frequencies of the system change with the applied load. In order to examine what happens, the natural frequencies of the system are calculated without load, then a static analysis with $P = P_{cr}/4$ is run, and a new set of frequencies are calculated. The procedure is repeated for $P = P_{cr}/2$. The results for the frequencies and corresponding periods are shown in table 3.2 below.

	P = 0	$P = P_{cr}/4$	$P = P_{cr}/2$
f_n (Hz)	0.013218	0.0114659	0.0093778
T_n (s)	75.65	87.21	106.63

Table 3.2: Natural frequencies and periods for the column

The eigenfrequencies decrease with an increasing load.

3.1.2 Element type

B32 elements are used for the column. They are three noded Timoshenko beam elements. Quadratic elements typically have a higher accuracy than linear elements, and it is often therefore sufficient with fewer elements. Linear elements in some cases also have problems with nonphysically high numerical stiffness. B33 elements are used for the dynamic part of the analysis of the column as they are more suitable for a dynamic analysis. The B33 element is a Euler-Bernoulli element with three nodes and three integration points per element.

It is used a quite big mesh, with an approximate element size of 1250 meters. The mesh dependency is low for this simple case, it is therefore chosen a big mesh to cut time costs. A very fine mesh is compared with the current mesh by comparing the buckling load for the two cases, and shows a difference in 0.153 %.

3.1.3 Material properties

The column is modelled with an E-module, $E = 2.1 \cdot 10^{11}\ \frac{N}{m^2}$ and Poisson ratio $\nu = 0.3$. To make the system into a one-degree-of-freedom-system the mass is lumped at the middle of the beam, and the mass density is set to $\rho = 0.1\ \frac{kg}{m^3}$. The natural period of the bridge is around T=100 s, from this the lumped mass is calculated to be $M = 4 \cdot 10^6$ kg. A dashpot is also included in the system, to make the structure go into steady state after just a few cycles. The damping ratio is set to be $\xi = 5$ %.

3.2 Arch model

For the second part of the assignment a curved beam is modelled as an arch with fixed ends and a uniformly distributed radial load in Abaqus.

3.2.1 Geometry

The arch is based on geometric data from the Bjørnafjord bridge, it has radius $r = 5000$ m and horizontal length $L_h = 4600$ m. This gives an arch height, or rise, f, of

$$f = r - \sqrt{r^2 - \left(\frac{L_h}{2}\right)^2} = 560 \text{ m}.$$

The cross section has the same parameters as for the column, see table 3.1, and the model is fixed at the ends and restricted against movement out of plane, see figure 3.2.

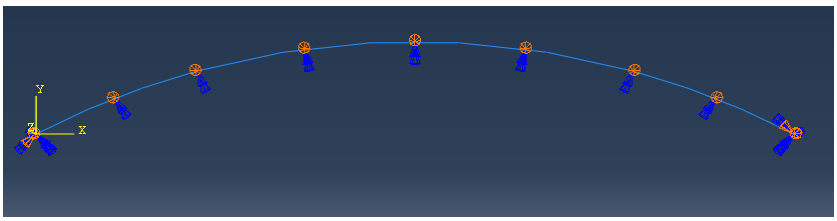

Figure 3.2: Arch with boundary conditions modelled in Abaqus

Similarly to the column, the eigenfrequencies of the arch change with the applied radially distributed load. In the following table, table 3.3, the eigenfrequencies and corresponding period for the first mode are presented.

	$P = 0$	$P = P_{cr}/4$	$P = P_{cr}/2$
f_n (rad/s)	0.0103	0.008895	0.007125
T_n (s)	97.087	112.423	140.351

Table 3.3: Eigenfrequencies and period for the arch corresponding to mode 1

Here, the eigenfrequencies decrease with increasing load.

3.2.2 Element type

For the arch the chosen element type is B32, the same as for the column. The model has 10 elements, each of which has a length of 460 meters.

3.2.3 Material properties

The arch has an effective mass of $\rho = 28000$ kg/m^3, and it has Rayleigh damping with damping coefficients $\alpha = 0.00754721$ and $\beta = 0.04178$. These values are calculated to get the correct damping ratio. To check the resulting damping of the model, a complex eigenvalue analysis is conducted in Abaqus, resulting in a damping ratio $\xi = 7.5\%$. This is a rather high damping ratio. The high effective mass was chosen to get the correct natural period of the system which should be around $T = 100s$.

3.3 Bridge model

In this section a simplified model of the Bjørnafjord bridge, modelled in Abaqus, is presented. The model itself has been created by PhD. Knut A. Kvåle. The real Bjørnafjord bridge consists of a floating part and a cable-stayed part; however, since we are mainly interested in the dynamic behaviour, only the floating part is included in the model. Since the bridge is a floating bridge the model includes the pontoons added as point masses and also the hydrodynamic forces from the waves acting on the model. The contributions from the pontoons are included in the Abaqus model using a WADAM analysis. Such an analysis provides the restoring stiffness and the pontoon inertia, it establishes the restoring stiffness based on the free-floating pontoons without the superstructure.

In the model, the following simplifications have been made:

- The cable-stayed section is disregarded, and the entire span of the bridge is floating.
- The height of the bridge is kept constant at the lowest height.
- The same pontoon type is assumed for all pontoons.
- The bridge is fully supported, both for translation and rotation, at both ends.

3.3.1 Geometry and material properties

The bridge model has a total arch length of 5525 meters, in the simplified model the pontoons are divided equally along this length. This gives an adjusted total number of pontoons as 54, since the pontoons are spaced roughly 102 meters apart on the real bridge. The parameters for both the geometry and the material properties are presented in table 3.4 below.

The effective mass in table 3.4 is included to account for the non-structural masses such as railings and asphalt, a mass of 17836 kg/m is distributed along the bridge girder giving $\rho_{\text{eff}} = 12472.73$ kg/m^3.

Along with the bridge model the steps used to calculate the effects from the pontoons was included. They are presented in the next paragraph.

Structure part	Description	Value
Pontoon	Length	58 m
	Height	9 m
	Width	10 m
	Area	558.5398 m^2
	Freeboard	4 m
	Draft	5 m
Girder beam	Second moment of area about axis n_1	2.68 m^4
	Second moment of area about axis n_2	115.62 m^4
	Cross-moment of area, axes n_1 and n_2	0
	Cross-sectional area	1.43 m^2
	Torsional constant	6.10 m^4
	Distance between beam axis and centroid	0.18 m
	Mass density	7800 kg/m^3
	Effective mass density	12472.73 kg/m^3
	Young's modulus	210 GPa
	Shear modulus	79 GPa
	Poisson ration	0.3
Column	Distance from pontoon top to girder bottom	7.920 m
	Distance from pontoon top to beam axis of girder	9.67 m
	Second moment of area about axis n_1	4.27029 m^4
	Second moment of area about axis n_2	4.27029 m^4
	Cross-moment of area, axes n_1 and n_2	0
	Cross-sectional area	0.671986 m^4
	Torsional constant	8.54058 m^4
	Mass density	7800 kg/m^3
	Young's modulus	210 GPa
	Shear modulus	79 GPa
	Poisson ration	0.3

Table 3.4: Geometric and material properties for the bridge model

To construct the model, a data file with the vital information (json-file), the required WADAM analysis, and a Python script are required. In the WADAM analysis the restoring stiffness from the pontoons are calculated without any superstructure. To adjust for this, the two values z_{cog} and $z_{cog,mod}$ in the json-file are used as follows

$$\widetilde{K}_{ii} = K_{ii} + \rho g V (z_{\text{cog}} - z_{\text{cog,mod}})$$

where K_{ii} refers to the original restoring stiffness, $\widetilde{K}_{ii}$ refers to the corresponding modified restoring stiffness, ρ is the water density, g is the gravitational constant, and V is the submerged volume.

The damping added to the model is from the pontoons with Rayleigh damping. To ensure the correct damping of the system a complex eigenvalue analysis is run in Abaqus. The damping of the system gives a damping ratio $\xi = 5\%$; which is equal to the target value.

3.3.2 Element type

For the bridge model a B31 element is used to model the bridge. This is a two node, linear Timoshenko beam element.

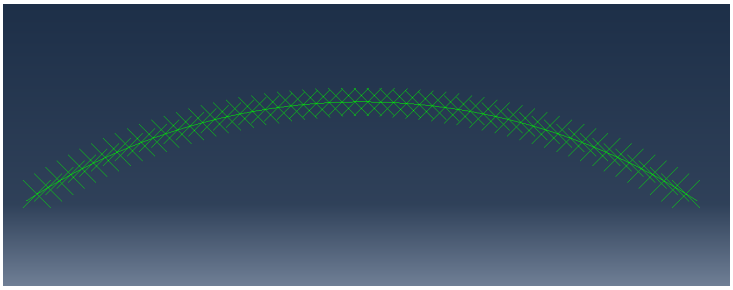

Figure 3.3: Bridge model

Figure 3.3 shows the bridge as modelled in Abaqus.

3.4 Column results

In this section the results from the analyses are presented both for the linear and nonlinear static case, and the dynamic case. For the linear case the buckling results are also compared against theoretical calculations. For the nonlinear cases the models may have an excessive displacement once buckling occurs. Hence, as a coarse limit, if the stress reaches yield stress the analysis stops. For more details on this limit, see appendix A.

3.4.1 Euler buckling

For a simply supported steel column with parameters as in table 3.1, Young's modulus $E = 2.1 \cdot 10^{11}\ \frac{N}{m^2}$, $I = 232.42\ m^4$ and length $L = 5000$ m the critical force, from equation 2.6, is

$$P_{cr} = \frac{\pi^2 EI}{L^2} = 19.27 \cdot 10^3 \text{ kN}.$$

Using a buckling analysis in Abaqus, the critical force is

$$P_{cr,Abaqus} = 19.28 \cdot 10^3 \text{ kN}.$$

The buckling modes for the column is shown in figure 3.4.

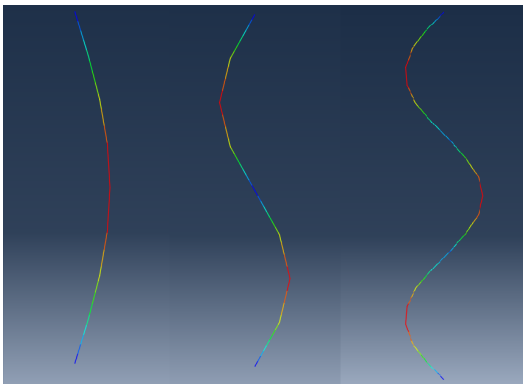

Figure 3.4: The three first buckling modes for the column

3.4.2 Nonlinear buckling

In this analysis the Riks method is used to solve the nonlinear buckling analysis. The column is exposed to a concentrated force at the columns top node.

The analysis is run with three different imperfections from the first mode. Abaqus gives a linear critical load $P_{cr} = 19.28 \cdot 10^3$ kN which is very close to the columns Euler load. The nonlinear results is shown in the graph below, see figure 3.5. It shows that the nonlinear buckling load is significantly lower than the linear buckling load for the cases with big imperfections. However, for the column with a small imperfection, the nonlinear buckling load is close to the linear buckling load.

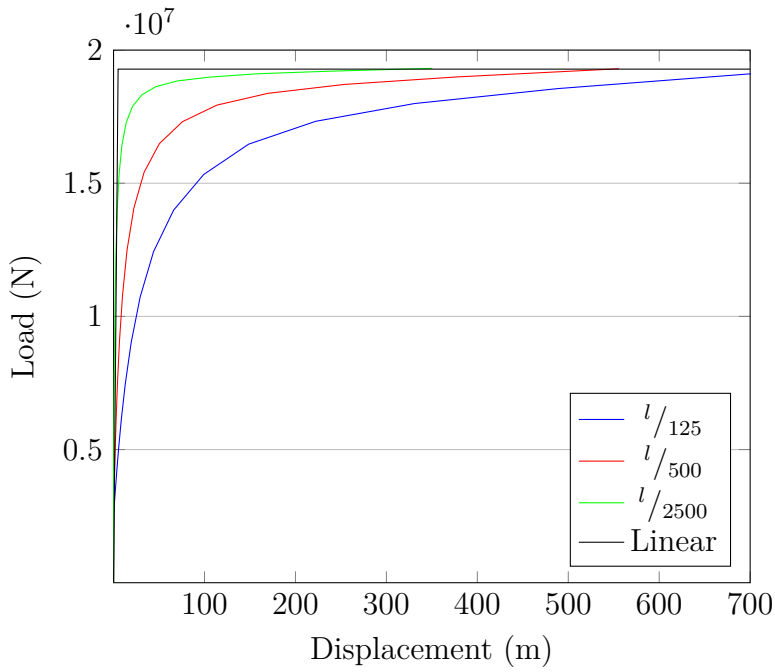

Figure 3.5: Plot showing how imperfections affect the buckling load

3.4.3 Dynamic buckling

For the case of dynamic buckling the analysis is run with a concentrated force at the top node of the column. The analysis is run in two steps, where the first step introduces a static load with half the magnitude of the total load. This step is included to make a deformation on the column to restrain the problem from becoming too nonlinear. The next step is the dynamic step, which is an implicit dynamic step where the dynamic load is introduced. This step is run with both the static load and the dynamic load to make the problem less nonlinear. Equation 3.2 show how the load is applied, where both a static load and a dynamic load is included. By adding a static load in addition to the dynamic load to the dynamic step the column will only be exposed for pressure. The tension part of the problem will go away as the two forces will zero each other out when the dynamic load originally would give tension in the model. If only the dynamic load of the problem would have been included the initial imperfection would have been straighten out, causing the stiffness of the column to be very high.

The load applied in the first static step can be written like the equation below:

$$P = \frac{\alpha P_{cr}}{2} \tag{3.1}$$

The applied load for the dynamic step, with both static and harmonic loading can be written as the following equation:

$$P(t) = \frac{\alpha P_{cr}}{2}\left(1 + \sin\left(\frac{2\pi}{T_L}t\right)\right) \tag{3.2}$$

Here α is the load factor, P_{cr} is the critical Euler load, T_L is the load period, and t is time. Figure 3.6 show the dynamic SDOF system used for the column.

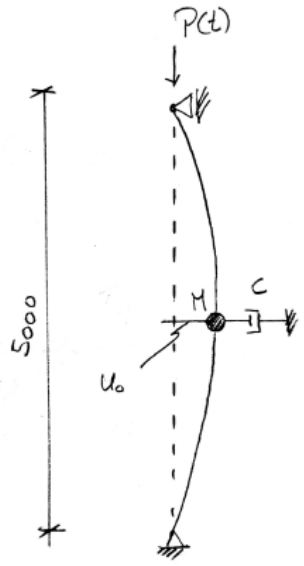

Figure 3.6: Illustration of the SDOF dynamic system

The dynamic buckling analysis is a nonlinear analysis, and imperfections from the first buckling mode is added to the column for a conservative analysis. The imperfection is set to $\frac{L}{50} = 100m$.

Mathieu's equation, equation 2.16 show that if ω is close to $2\omega_n$ the amplitude of oscillations will exponentially increase with time.

For the slender column both a point in the stable and the unstable areas are tested, figure 3.7. The graphs below show how the deformation grows exponentially for the unstable point, figure 3.8b. For the point in the stable region, the structure goes into steady state, figure 3.8a.

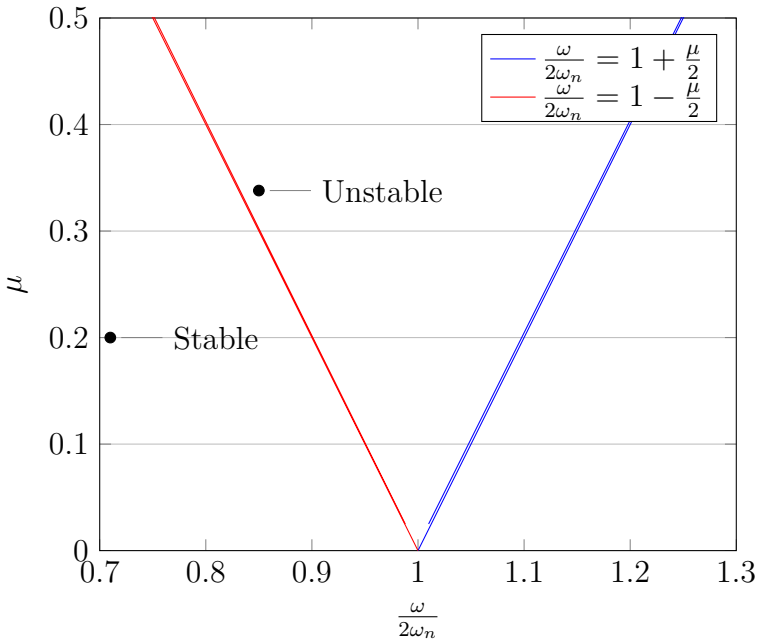

Figure 3.7: First instability region

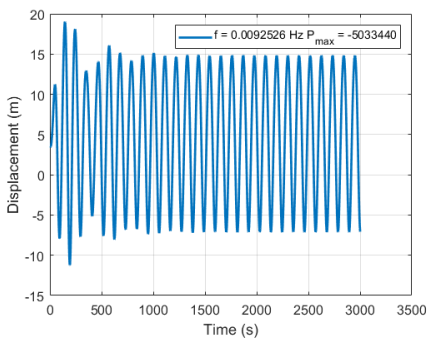

(a) Stable plot

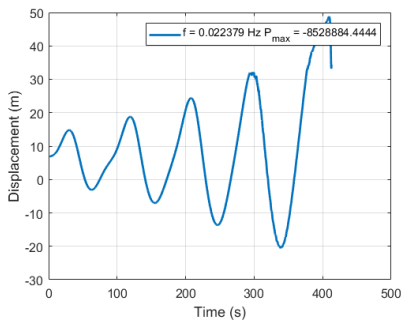

(b) Unstable plot

Figure 3.8: Stable and unstable plots for the column

To determine relationship between the load frequency, load and displacement at the midpoint several analyses are required. In order to run the Abaqus analysis several time, a MATLAB-script has been created. It uses an input file from Abaqus, runs the analysis and post-processes the results. The "Abaqus2matlab"-scripts are made by George Papazafeiropoulos [18]. Figure 3.9 shows the process of the MATLAB-script, and the script itself can be found in appendix B

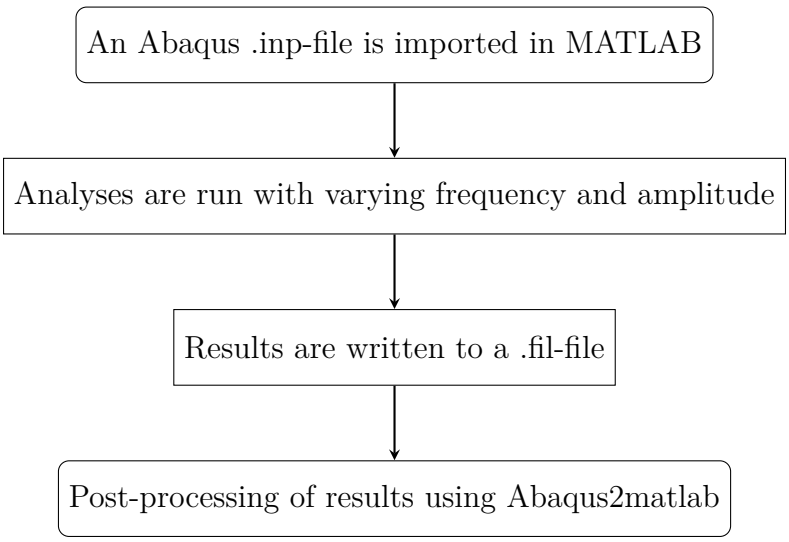

Figure 3.9: Flowchart showing the process of the MATLAB-script

The analysis was run 300 times for 10 different loads with $\alpha \in [0.4, 0.7]$, and 30 different frequencies, $\omega \in [0.7\omega_n, 2.5\omega_n]$. The analysis was run for 3000 seconds to ensure that the unstable cases would diverge before the analysis was over, and that the stable cases would reach steady state. The displacement is collected from the last part of the analysis, after the stable cases have gone in to steady state. This is to make it easier to see the relationship between the displacement, the load frequency and the load. To ensure correct output data the initial increment time step is set to 0.02 seconds and maximum time step equal to 0.5 seconds. The small time-steps and the long time period makes the analyses time-consuming, and takes two to three days to complete.

Figure 3.10 and 3.11 shows the resulting plot from the analyses. Figure 3.10 is the maximum displacement at the midpoint for the different combinations of load frequency and load, making the unstable areas yellow. This shows how the unstable areas corresponds to parametric resonance around double the natural frequency, $f = 0.026$ Hz, which correspond with the theory. The plot also shows how the column gets unstable in the area around the natural frequency, $f = 0.013$ Hz.

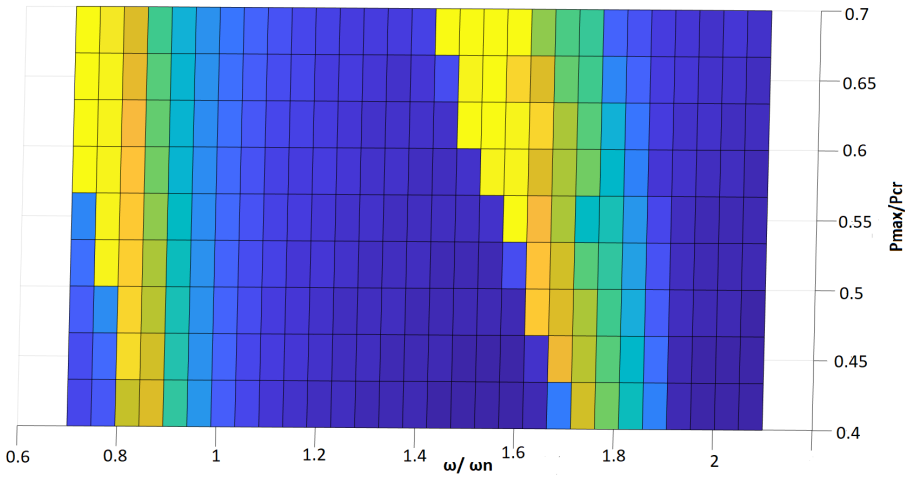

Figure 3.10: Unstable areas for the column

As seen in table 3.2, the eigenfrequencies change with applied load. This is the reason that the regions in figure 3.10 curve towards the left. The unstable areas in the figure above does not correspond with the natural frequency and double the natural frequency, as this is plotted against the natural frequency of the column without any static loading.

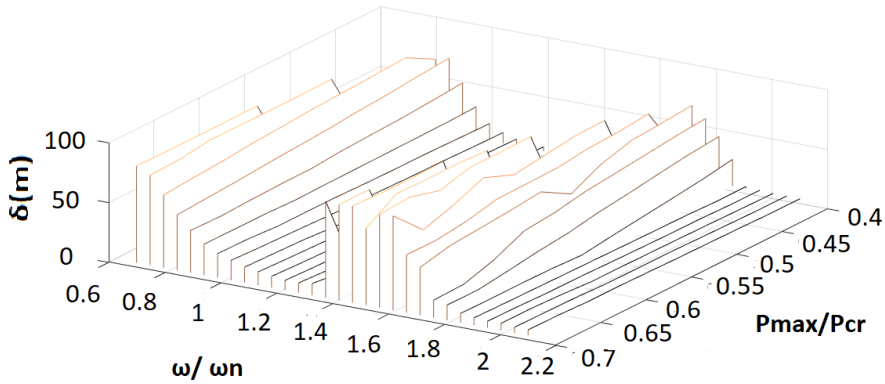

Figure 3.11: Plot showing the relation between frequency, load-amplitude and displacement.

3.5 Arch results

In this section the results for the arch are presented. Both for the static cases and the dynamic cases. In the dynamic case, a similar cut-off criterion has been implemented as that for the column.

3.5.1 Euler buckling

Using Abaqus to perform a linear buckling analysis of an arch with geometric parameters as in section 3.2.1 the critical load for the first mode is

$$\mathrm{q}_{cr} = 34400 \text{ N/m}.$$

Using theoretical results, equation 2.9 and table 2.1, the critical load is $\mathrm{q}_{cr} = 28629.574$ N/m. This is lower than the load from Abaqus; however, the analytical results are calculated for an arch with a central angle $\alpha = 30°$, whereas the arch in Abaqus has $\alpha = 27.385°$. From table 2.1 n decreases with an increasing angle α, this causes the critical load to also decrease. Hence, since the Abaqus model has a smaller angle it will give a larger critical load. As a simple estimate for the value of n, polynomial interpolation gives $n = 9.316$ and a corresponding critical load $q_{cr} = 33497.202$ N/m. The error between this estimate and the Abaqus result is then 2.6%. Figures 3.12a, 3.12b and 3.12c show the three first buckling modes for the arch.

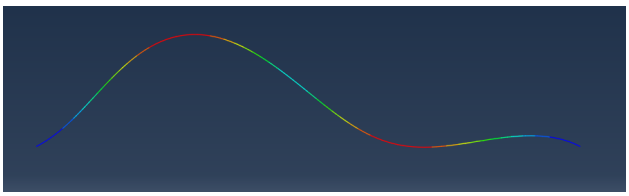

(a) First buckling mode

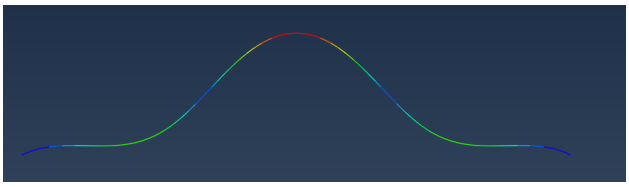

(b) Second buckling mode

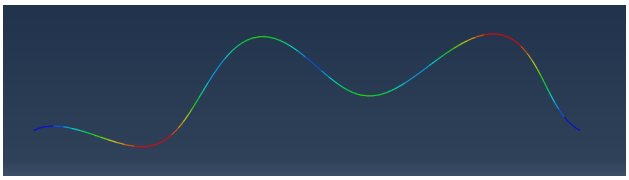

(c) Third buckling mode

Figure 3.12: The three first buckling modes

3.5.2 Nonlinear buckling

Similarly to the column analysis, the nonlinear buckling analysis for the arch is run with the Static, Riks method. The analysis is run for two cases with imperfections collected from the first mode shape; then one analysis is run without imperfections. The buckling modes are shown in figure 3.13 and figure 3.14. The imperfections in the nonlinear buckling analyses are, $\frac{l_h}{350} = 18.4m$ and $\frac{l_h}{1000} = 4.6m$.

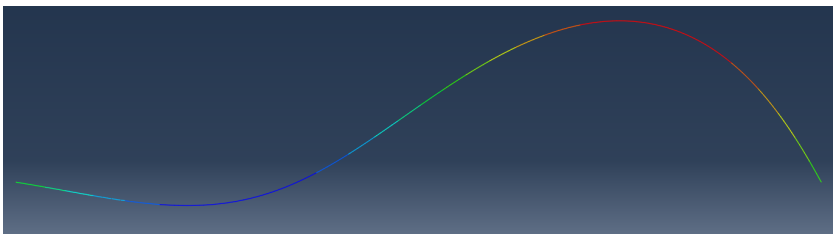

Figure 3.13: Asymmetric buckling mode

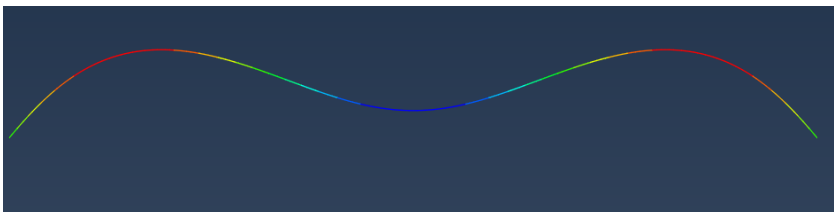

Figure 3.14: Symmetric buckling mode

The results from the nonlinear bucking analysis show that the critical load is reduced for the cases that includes imperfections. However, the results from the nonlinear case with small imperfections show that the critical load is about the same as for the linear case. Figure 3.15 show the LPF-displacement curve for the two cases. The load proportionality factor (LPF) is the ratio between the applied load and the linear buckling load. The asymmetric cases has a much lower buckling load than the snap-through case. The load proportionality factor shows that for snap-through buckling to occur the load must be about 50% higher than for linear buckling.

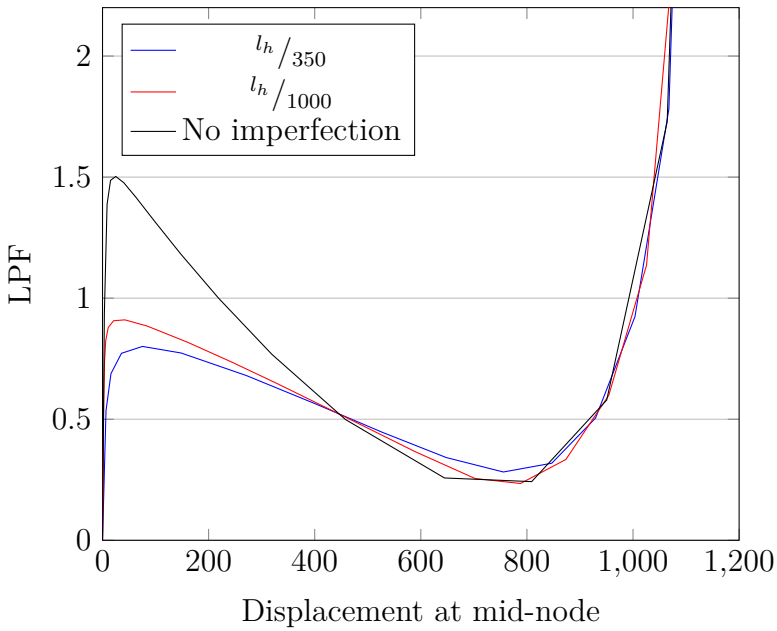

Figure 3.15: Load-displacement curve

3.5.3 Dynamic buckling

The dynamic buckling analysis for the arch is quite similar to the case for the column. The analysis is run over two steps, first a linear static step, then a dynamic implicit step. The dynamic step is run with both a harmonic load, and a static load. The static load is simulating the mean wind, that would be a part of the analysis for the bridge, and prevents tension in the model. The applied load for the arch in the dynamic step can be written as follows:

$$q(t) = \frac{\alpha q_{cr}}{2}\left(1 + \sin\left(\frac{2\pi}{T_L}t\right)\right) \tag{3.3}$$

Where q_{cr} is the critical radial distributed load, α is the load factor, T_L is the natural period for the arch without the static load, and t is the time.

Imperfections are included from the first mode of linear buckling, with a ratio $\frac{l_h}{350} = 18.4m$.The imperfections are included to make a conservative system. The dynamic buckling analysis is a nonlinear analysis, and includes geometric nonlinearities.

The MATLAB-script created for the arch is quite similar to the one for the column. The analyses are run for 5000 seconds. The displacement data is plotted from a node on the left side of the arch, about a quarter distance from the end, to get the maximum displacement as the arch will deform asymmetrically. The analysis is run 350 times with 10 different load factors, $\alpha \in [0.4, 0.7]$, and 35 different frequencies, $\omega \in [0.3\omega_n, 2.7\omega_n]$. The results are plotted in figure 3.16. The plot shows that the arch does not get unstable around double the natural frequency for the lowest loads; this is because of the high damping in the system.

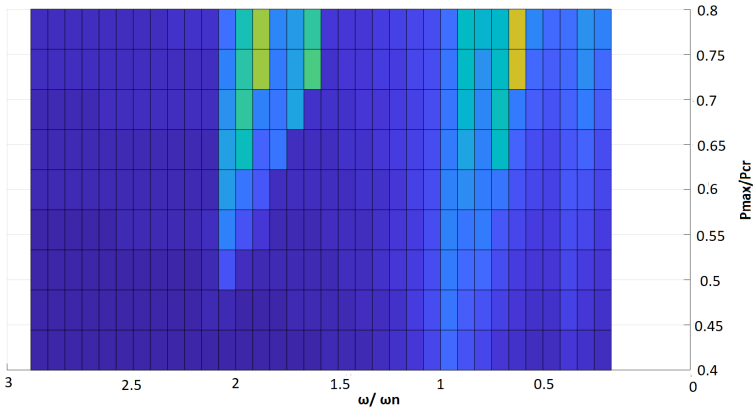

Figure 3.16: Unstable areas for the arch

To better see how the unstable areas depend on the frequency a set of analyses with frequencies $\omega \in [0.5\omega_n, 3\omega_n]$ and load amplitude with $P_{max} = 0.4P_{cr}$ and $P_{max} = 0.7P_{cr}$ is run. In total 60 different analyses are run with 30 different frequencies and 2 different load amplitudes. Figure 3.17 illustrates how the displacement increases in the unstable areas around the natural frequency, ω_n and around double the natural frequency, $2\omega_n$.

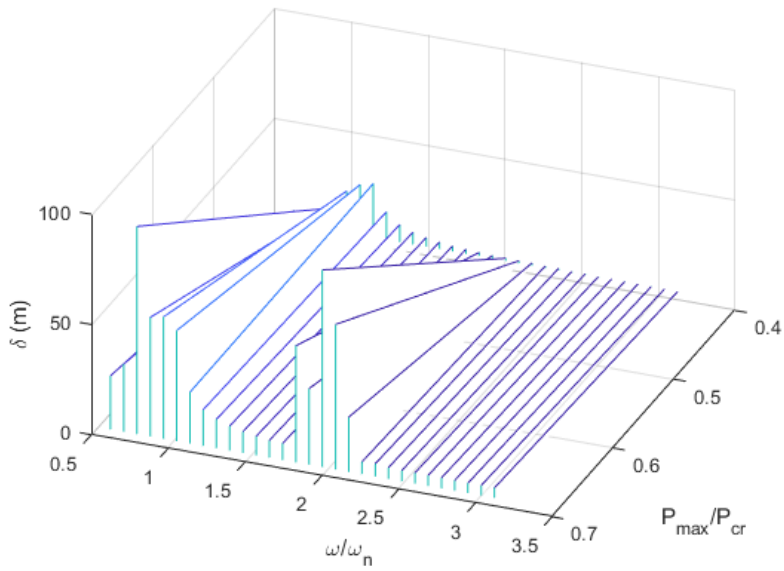

Figure 3.17: Plot showing the relation between frequency, load-amplitude and displacement.

Figure 3.16 shows the instability areas for the arch, and the instability areas are tilted towards the lower frequencies. The static load applied in the first step of the analysis gives a reduction of the natural frequency. This means that the applied load will give resonance in lower frequencies than the actual natural frequency as the load increases.

When the static loading is applied it changes the behaviour of the system. Figures 3.18b and 3.18a below show the time-series for two analysis. In figure 3.18b the static load is about 1.5 times as large as the load in figure 3.18a; otherwise the systems are the same, both regarding dynamic load and load frequency. In one of the analysis the arch becomes unstable because of parametric excitation, but in the other analysis the arch goes in to steady state.

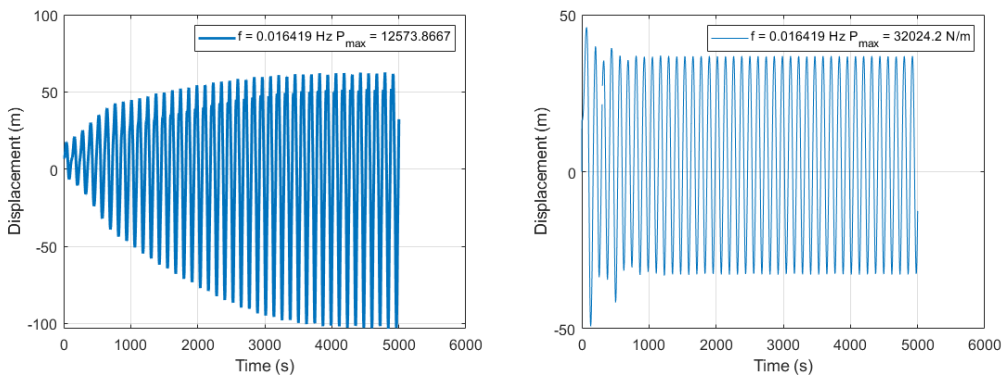

(a) Unstable analysis (b) Stable analysis

Figure 3.18: Displacement-plots for the arch showing the difference in static load

Two time-series from a stable and an unstable analysis are shown in figures 3.19a and 3.19b respectively. The unstable plot is collected from $\omega = 2.1\omega_n$ with applied load $q = 0.7q_{cr}$ in the unstable area, and the stable plot is collected from $\omega = 2.6\omega_n$ with applied load $q = 0.5q_{cr}$ in the stable area.

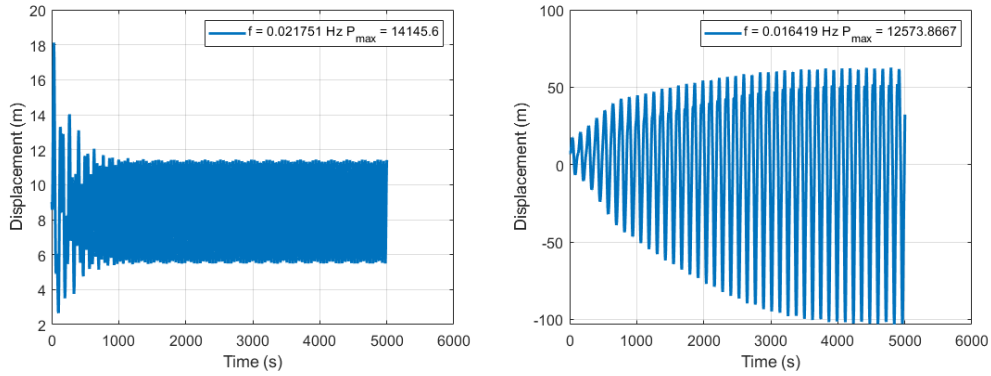

(a) Stable analysis (b) Unstable analysis

Figure 3.19: Displacement-plots for a stable and an unstable analysis

The external power added to the system and the dissipation of power from viscous dissipation for the analyses above are plotted in figure 3.20. As the deformation keeps growing for the unstable analysis the external work will increase by a higher ratio than the viscous dissipation, this results in the external power being higher than the power dissipated as seen in figure 3.20b. For the stable case the external work and the viscous dissipation are increasing by the same ratio. The external power and the dissipated power which is the derivative of the energy gives straight curve, resulting in a steady power-plot 3.20a.

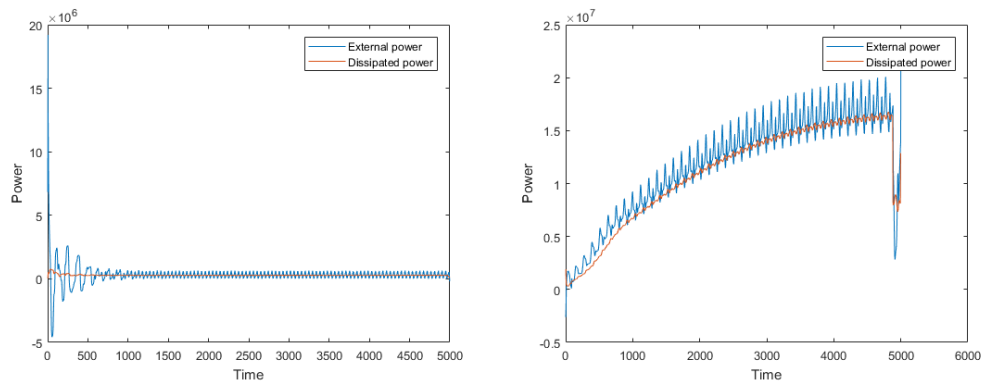

(a) Stable analysis (b) Unstable analysis

Figure 3.20: External work and viscous dissipation plotted for the two analyses

As the loading on the bridge will not be harmonic, a series of stochastic analysis has also been run for the arch. To investigate what happens in the unstable areas when the load is stochastic, the harmonic load is replaced by a random load. The random loading is run for load-spectres in the unstable region $\omega \approx 2\omega_n$, with different bandwidths.

For the first case the standard deviation is set equal to $\sigma = 0.3P_{cr}$, and the bandwidth is equal to $B = 0.001$. This makes the maximum spectral density, $S_{xx} = \frac{\sigma^2}{B}$. By having a very narrow bandwidth the loading will almost be harmonic, making the stochastic loading results easier to interpret. The analysis also includes a static load in both the dynamic and the static step for this simulation. The static load is equal to 35% of the Euler buckling load, $P_{static} = 0.35P_{cr}$; this results in a total load of around 80% of the Euler buckling load, this is a rather high load that was chosen to make sure the analysis with the lowest bandwidth would experience parametric resonance. In figure 3.21b the load spectrum is shown, and the dynamic load time-series is shown in figure 3.21a.

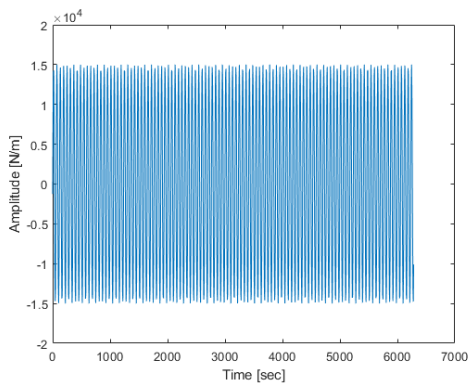

(a) Time-series

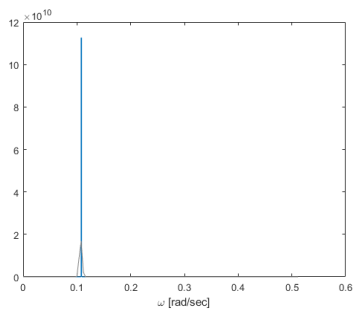

(b) Load spectrum

Figure 3.21: Time-series and the corresponding load spectrum for a stochastic load with a very narrow bandwidth

The resulting time-series for the arch exposed to a stochastic narrow banded load is shown in figure 3.22a below, this shows how the response is quite similar to the response from the harmonic loading, see figure 3.19b. The power-plot in figure 3.22b shows that while the displacement grows rapidly in the beginning of the analysis the external work grows with a higher ratio than the viscous dissipation for a large amount of time. This means that the energy transferred in to the system is higher than what can be damped out, and results in high deformations.

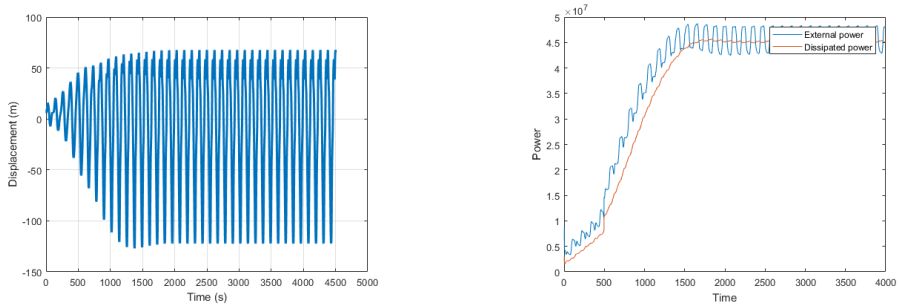

(a) Displacement-plot for arch with stochastic load with narrow bandwidth

(b) External power and dissipated power

Figure 3.22: Displacement-plot and the corresponding power-plot of an unstable stochastic analysis

Several analyses were run to establish at which bandwidth parametric resonance no longer would occur. The analyses were run with the same parameters as mentioned earlier in this chapter. The bandwidth was increased until the loading was represented by a somewhat steady time-series, with as narrow a bandwidth as possible. The maximum bandwidth was calculated to $B = 0.21$, after this point the analyses would no longer be narrow banded. In order to determine whether resonance did occur or not, the external power added to the system and the dissipated power from viscous dissipation was plotted.

Analyses with bandwidths $B \in [0.02, 0.21]$ were run and not any of the resulting plots did show any sign of parametric resonance. As the dissipated energy never were below the external work energy for a longer period of time. One of the resulting plots are displayed in the figures below, these plots are representative for the other analyses in the range mentioned above. Figure 3.23a shows the displacement-plot for the stochastic analysis with bandwidth $B = 0.15$ and figure 3.23b shows the corresponding energy-plot.

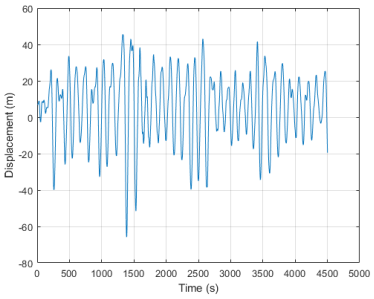

(a) Displacement-plot for arch with stochastic load with bandwidth B=0.15

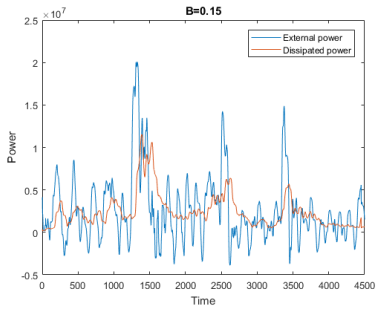

(b) External power and viscous dissipation

Figure 3.23: Displacement-plot and the corresponding power-plot for a stochastic analysis

The time-series for the load is displayed in figure 3.24 below. In addition to this load the static load is also a part of the analysis.

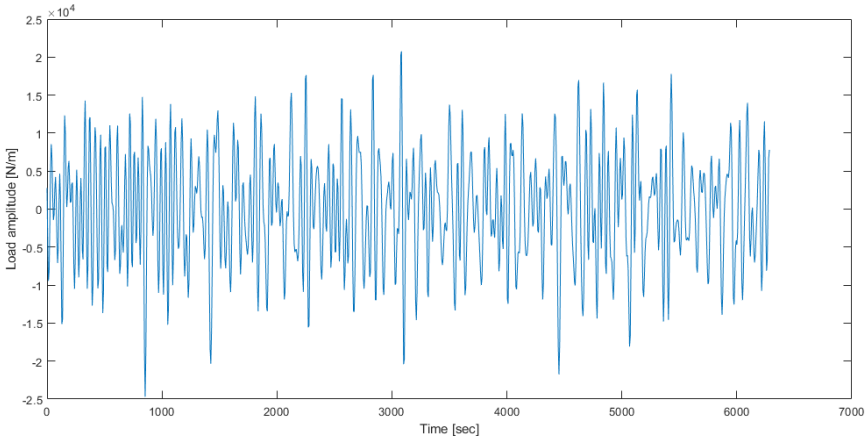

Figure 3.24: Time-series for the stochastic loading with bandwidth B=0.15

In some of the load cases the deformations get rather large, some around 100 meters. However, these systems do not show any sign of an occurring resonance phenomenon. For a more complete set of plots see appendix D.

3.6 Bridge results

In this section the results from the analyses of the simplified bridge model is presented. This model has been subjected to similar analyses as for the column and the arch.

3.6.1 Linear buckling

The linear buckling load for the bridge was calculated for the first mode and with a radially applied distributed load, similar to the arch. This resulted in the critical load below:

$$P_{cr} = 13006 \, \frac{N}{m}$$

The first buckling mode for the bridge model corresponds with the first buckling mode for the arch in the previous chapter. Figure 3.25 shows the first buckling mode for the bridge model.

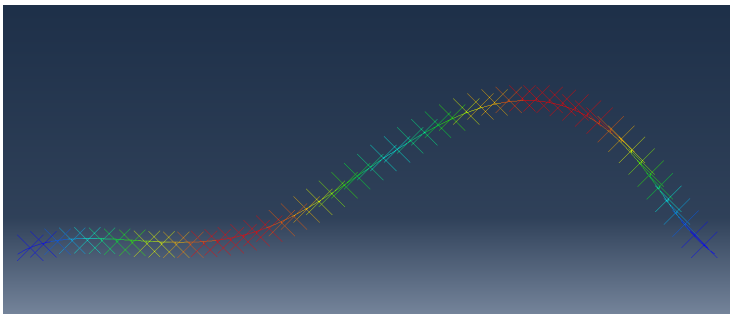

Figure 3.25: First buckling mode for the bridge

3.6.2 Nonlinear buckling

A nonlinear buckling analysis was run using the Static Riks method. The analysis was run with three different imperfections from the first mode of linear buckling, $\frac{l_h}{100} = 54.4m$ $\frac{l_h}{200} = 27.2m$ and $\frac{l_h}{2000} = 2.7m$. The resulting load-deformation-plot is shown in figure 3.26. By including imperfections the buckling load decreases.

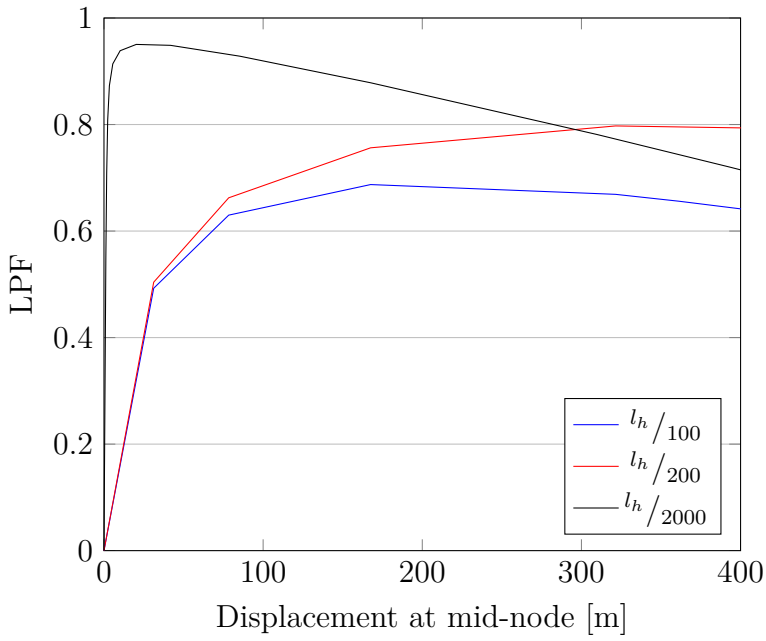

Figure 3.26: Load-displacement curve

3.6.3 Dynamic buckling

The dynamic buckling analysis for the bridge was run similarly to the dynamic buckling analysis for the arch. The MATLAB-script was adjusted to the new model, and run with the new inp-file. The static and dynamic step for the bridge is exactly the same as for the arch model. The applied loading for the dynamic part of the analysis is similar to the load applied on the arch, see equation 3.3. An additional step is added for the bridge analysis to include the uplifting of the pontoons, and the gravity forces. The model was also set to include imperfections from the first buckling mode with an imperfection of 25 meters. The dynamic buckling analysis does also include geometric nonlinearities.

The main concern for the bridge is to establish which frequencies that makes the bridge unstable. To set focus on the frequencies the MATLAB-script was set to run 30 different load frequencies in the range $\omega \in [0.3\omega_n, 2.2\omega_n]$. The applied load amplitude is set to $0.4P_{cr}$ and $0.7P_{cr}$. The dynamic part of the analysis are run for 5500 seconds.

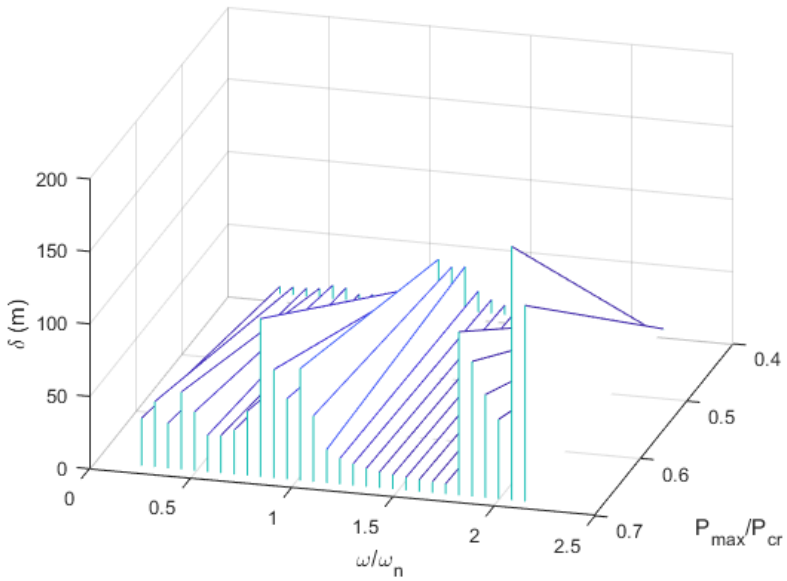

Figure 3.27: Instability area for the bridge

Figure 3.27 shows the results from the analysis with 30 different load frequencies, and two different load amplitudes for the bridge. Displacement-plots for a stable and an unstable analysis are displayed in figure 3.28a and 3.28b.

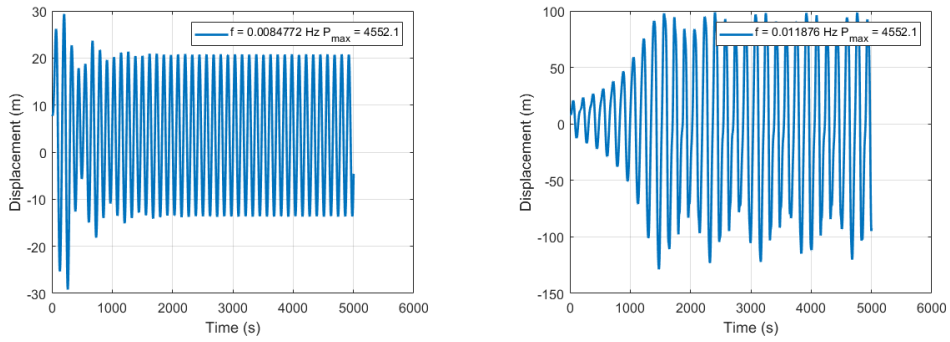

(a) In the stable area (b) In the unstable area

Figure 3.28: Time-series for the bridge

The wave loading on the Bjørnafjord bridge is a high-frequency load with a shorter period than what have been reported earlier in this chapter. A new analysis was run to establish how the bridge responds to high-frequency loading, and to detect any unstable areas for this type of loading. For the Bjørnafjord bridge the typical period for the wave-loading are around $5s$, whereas the period of the bridge itself is around 100 s.

According to Sha et. al [19] the first-order wave force dominates the frequency range from 0.1 to 0.25 Hz. To check this range analyses have been run with frequencies ranging from 0.1 to 0.5 Hz and the load amplitude was in the range $P \in [0.4P_{cr}, 0.7P_{cr}]$. The results of which can be found in figure 3.29a below.

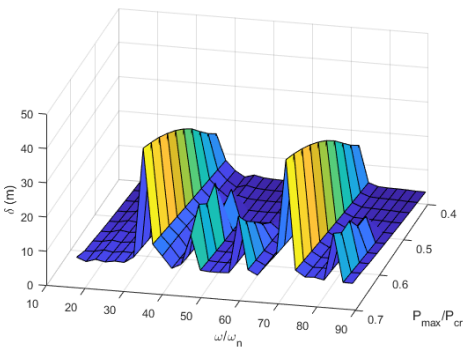

(a) Instability area for the bridge for $f \in [0.1, 0.5]$

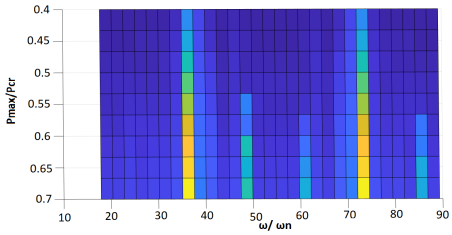

(b) Force plotted against frequency

Figure 3.29: Plot of the higher frequencies for the bridge

Figure 3.29b shows that the model has resonant behaviour at around 35 times and 72 times the natural frequency for the whole load range. It also has some minor peaks at around 48, 61 and 86 times the natural frequency for loads in excess of $0.55P_{cr}$.

Like the arch model, stochastic analyses have been run for the bridge to see how the bridge model responds to the stochastic loading. The stochastic analyses for the bridge are similar to the stochastic analyses for the arch, with standard deviation $\sigma = 0.3P_{cr}$, and maximum spectral density $S_x = \frac{\sigma^2}{B}$. First a load with a very narrow bandwidth was tested to establish that the bridge responds as expected. The results are presented in figure 3.30 below.

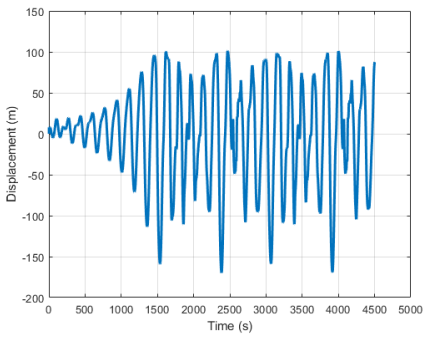

(a) Unstable by stochastic loading

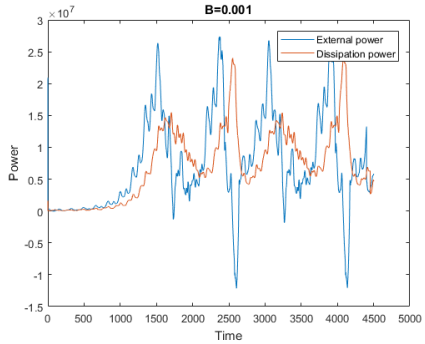

(b) External power and dissipated power

Figure 3.30: Deformation-plot and corresponding power-plot for the unstable bridge model

Then analyses with stochastic load with bandwidths in the range $B \in [0.03, 0.15]$ were run. The maximum bandwidth was calculated to 0.15 as this is the bandwidth where the load spectrum crosses the y-axis. Some of the analyses with a narrow bandwidth did show signs of parametric excitation when the external energy increased more than the viscous dissipation for a longer period of time, and the external power was quite high for some cases; this occurred for a bandwidth up to $B = 0.1$. Figure 3.31 shows the displacement-plot and the power-plot for one of these analyses, $B = 0.08$. The rest can be found in appendix D. This can also be seen in the deformation-plot as increasing displacements.

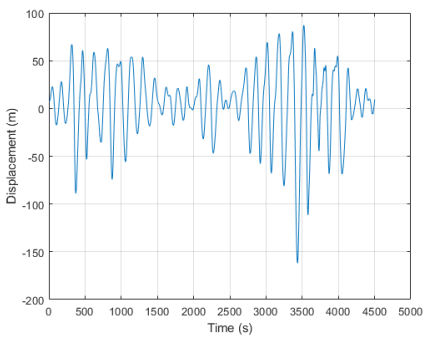

(a) Unstable by stochastic loading

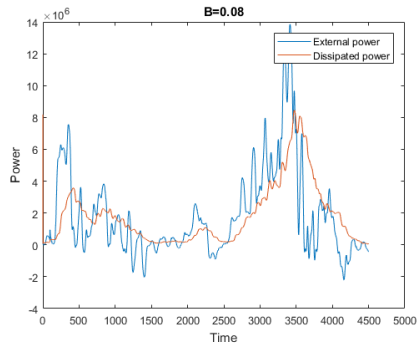

(b) External power and viscous dissipation

Figure 3.31: Deformation-plot and corresponding power-plot for the unstable bridge model for B=0.08

Time-series for the stochastic analysis with $B = 0.08$ and $B = 0.14$ are displayed in the figure 3.32 below. This loading comes in addition to the static load in the dynamic step which is equal to $P_{static} = 4552\frac{N}{m}$, 35% of the Euler buckling load.

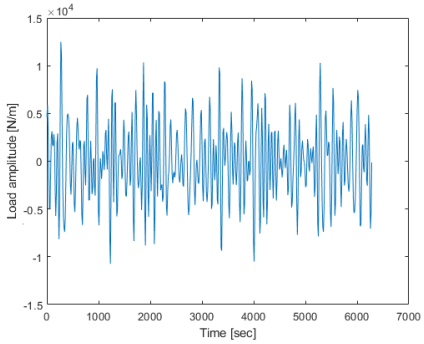

(a) Time-series for the stochastic analysis with bandwidth B=0.08

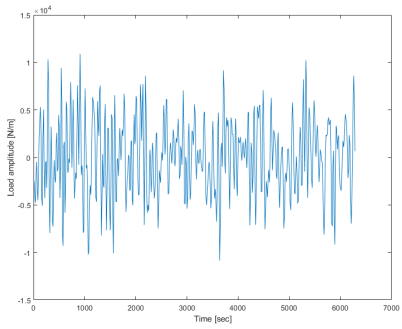

(b) Time-series for the stochastic analysis with bandwidth B=0.14

Figure 3.32

Some of the analyses run with higher bandwidths does also have sudden high peaks of power, resulting in high peaks in the deformation-plot. Figure 3.33 shows the plot for the stochastic process with a bandwidth $B = 0.14$.

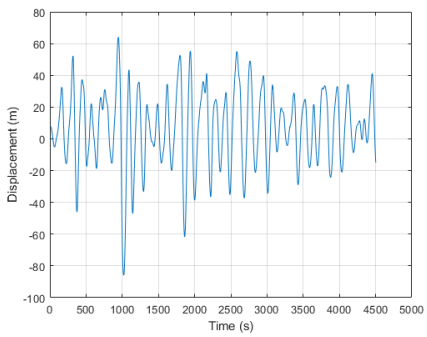

(a) High deformation peaks by stochastic load

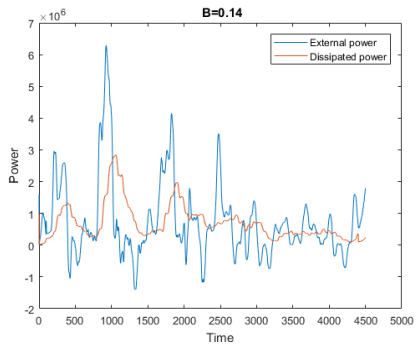

(b) External power and dissipated power

Figure 3.33: Deformation-plot and corresponding power-plot for the bridge model with high peaks in external power for B=0.14

Chapter 4

Discussion

In this section the results from the analyses are discussed. First for the simple column, secondly for the simple arch and finally for the simplified bridge model. In all the cases, several analyses were run using both MATLAB and Abaqus. A harmonic dynamic load was applied in all three cases, and a stochastic load was also tested for the arch and the bridge. The stochastic load is representative of the natural wave load which the real bridge will be subjected to. The stochastical analyses have been run using only one randomly generated load for each bandwidth, this has been done due to time constraints. In order to improve these results, several random loads should have been generated, say 20 for each bandwidth, and an average load should have been calculated based on these. The average load should then have been used to run the analyses.

For the column and the arch, the critical linear buckling load has been calculated both analytically and with Abaqus. In the case of the column, the two results are an almost perfect match, only an error of 0.052%, whereas for the arch there is a larger discrepancy due to the fact that the theoretical results and Abaqus results are calculated using a different central angle.

Column

The simple column is modelled as a massless beam with a point mass at the midpoint. This makes the model a single degree of freedom system, and the dynamic effects are easier to interpret. One thing to note is that for such a system, the geometric imperfections have a significant impact on the buckling load. The larger the imperfections the smaller the buckling load.

As a simple check of the model, the linear buckling load from Abaqus is compared with a theoretical result. Abaqus gives $N_{cr} = 19.28 \cdot 10^3$ N and the theoretical result is $N_{cr} = 19.27 \cdot 10^3$ N. The discrepancy is only 0.05%; hence, the model has a very good agreement with the theory.

Even though the column is modelled as a simple system as possible it presented several unexpected difficulties. In the first attempt the column was modelled without a static load, just a harmonic dynamic load. This caused problems since the harmonic load caused the column to be exposed to tension which changed the stiffness of the system, and caused the problem to become highly nonlinear. To deal with this problem a static load was applied prior to the dynamic load. However, by applying a static load the natural frequency of the system change depending on the static load. An increasing static load lowers the natural frequency, as seen in table 3.2. The frequencies are lowered since by applying the static load the stiffness of the system decreases.

For the column the natural frequency of the system is $f_n = 0.013$ Hz. After running several analyses the system exhibits resonant behaviour both at the natural frequency and at double the natural frequency. The first case is to be expected as this is the regular resonance phenomena, however at double frequency parametric resonance occurs. Figure 3.10 shows the unstable areas for the column. The unstable areas are curved due to the applied static loading, which causes the natural frequency to change.

Arch

Initially the arch was modelled using two point masses, each located a quarter distance from each end. This was done to create as simple a system as possible. However, when running analyses this created some complications with the results. For some frequencies the deformations became unreasonably large. Due to these complications the decision was made to use a distributed mass instead. Also, the damping ratio for the arch is set to $\xi = 7.5\%$, which is a rather high damping. This is done in order to dampen out interference from different modes, that is, to make the response easier to interpret.

Similarly to the column, the buckling load for the arch is compared against theoretical results. Using polynomial interpolation to estimate the root value corresponding to $\alpha = 27.385°$; the theoretical buckling load is $q_{cr} = 33497.202$ N/m. Abaqus gives a buckling load of $q_{cr} = 34400$ N/m. The error between these two results is 2.6%; hence, the arch model agrees well with the theoretical result.

The arch was chosen as a basic representation of the bridge, and separate analyses were run using harmonic load as the dynamic load and stochastic load as the dynamic load. The asymmetric mode is excited at a much lower load and it is the one that has been used in the subsequent analyses. For the arch, figure 3.16 show the results of the harmonic analyses. Similar to the column, the system exhibits resonant behaviour at both the natural frequency and double the natural frequency.

For the stochastic load, analyses were first run with a very narrow bandwidth as this will be similar to harmonic load. The bandwidth was then increased in order to see if there was a point at which parametric resonance no longer would occur. The bandwidth had to be increased until the point where the load was a steady load, similar to the loading the bridge would be exposed for, and to be able to interpret the results. Stochastic loading from wind and waves are highly irregular by nature. If the bandwidth is too narrow the load will act as a sum of harmonic components with almost the same frequency. Hence, this will not be a proper representation of the loads. By analysing the energy of the system, a criterion for which bandwidth could give a stable system was established. If the energy in the system increased more than the energy caused by damping then the system would become unstable.

With a very narrow bandwidth turning the force into what is very similar to a harmonic force the arch became unstable. The power plot in figure 3.22b shows that the external energy is increasing with a steeper slope than the viscous dissipation for a large amount of time in the beginning of the analysis; this enables the arch to get very high deformations. With a broader bandwidth the arch did not get unstable according to our analyses, this may be because the loading was not high enough for a large enough amount of time. This enables the external power to decrease before the arch gets unstable. The power plots for the stochastic analyses does show that the external power is higher than the viscous dissipation for some amount of time, but the energy quickly returns into balance. Some of the analyses show that the arch gets very high displacement caused by a sudden high increase of power. The results are all based on one analysis on each bandwidth as this is a random load its hard to define a bandwidth where parametric resonance does not occur, as it should have been run several analyses making an ensemble average.

The analyses also show how the damping of the system affects the instability regions. As seen in figure 3.16, the system has a rather high damping. This causes the parametric resonance from the lower loads to be damped out; this is seen as the instability regions are raised above the horizontal axis in the plot. This may also have impacted the stochastic analyses as to why none of them experienced parametric resonance.

Bridge

For the simplified bridge model, both harmonic and stochastic loading were tested. Figure 3.27 show the results for the harmonic load. The resulting plot show that frequencies near the natural frequencies and double the natural frequencies gives a higher deformation, and the model becomes unstable. The bridge model was also tested for frequencies which are similar to the waves at Bjørnafjorden. These results are presented in figure 3.29a. In this plot resonant behaviour is still present at the higher frequencies. Two areas in particular may cause problems, that is around 35 and 72 times the natural frequency. One thing also to note is that by increasing the load, regions which was previously stable may become unstable. This is represented as the minor peaks appearing around at around 47,57 and 82 times the natural frequency in 3.29a. Also, the unstable areas are quite narrow; this is an inherit trait of Mathieu's equation, equation 2.16. The higher the

multiple of the natural frequency, the narrower the area.

The stochastic analyses for the bridge resulted in plots with high deformations and some where parametric resonance occurred. Parametric excitation happens with the lower bandwidths where the load amplitude has longer periods with high peaks. Similar to the arch only one analysis is run for each bandwidth making it hard to define whether or not this happens for all analysis run with the bandwidth as the loading is random. It does however show that the possibility for parametric excitation is there, and that high deformations may occur. These analysis was also run with a rather high loading, the standard deviation was set to $\sigma = 0.3P_{cr}$ and with the static load $P_{\text{static}} = 4552\frac{N}{m}$ which is 35% of the Euler buckling load in addition. The total load exceeds the Euler buckling load at some points during the analysis, and with the imperfections included in this analysis the buckling load is decreased to between 70% and 80% of the Euler buckling load. This gives a loading well above the buckling load for the bridge and the high deformations is for this reason expected.

Chapter 5

Conclusion

For all three systems, resonance has occurred at around the natural frequency and parametric resonance around double the natural frequency as expected.

One important thing to note is that static loads significantly change the frequencies of the system. For the cases presented in previous chapters, the eigenfrequencies decrease with an applied static load. Resonance may therefore occur at frequencies which are lower than one could expect from the dynamic system on its own.

The stochastic analyses show that the bridge may experience high deformations and parametric resonance even with a random load. As mentioned in the previous chapter 4, the analyses were only run one time with each bandwidth and it is for this reason hard to conclude that bandwidths below $B = 0.1$ will result in parametric excitation for all loads with these bandwidths. It can however be concluded with that high deformations and parametric excitation did occur in these analyses when the load frequency was $w \approx 2w_n$ and it may result in problems for the bridge.

Chapter 6

Further work

This thesis is based on very simplified models, and the model most similar to the actual bridge does also have some simplifications. To really see how the bridge will respond to the dynamic loading with regard to dynamic buckling, the analyses should be run on a model without the simplifications mentioned in section 3.3.

A part of the thesis was also focused on the behaviour of the models exposed for stochastic loading in the unstable areas; this loading was based on a standard rectangular load spectrum. To better examine how the bridge responds to the actual stochastic loading a better suited load spectra could be tested, for instance the JONSWAP-spectra would give a more accurate result. Certain limitations was also set on the bandwidth, it could also be interesting to examine different bandwidths to see if the arch and the bridge behaves any differently, and if parametric excitation occur. An important task would also be to run several stochastic analyses to make an ensemble average. This will make it easier to define whether or not the bridge may get unstable by dynamic buckling with random loading.

During our work on this thesis another issue was discussed, this was the issue of double harmonics. By applying two different harmonic loads the system may respond differently, and the issue of parametric excitation may disappear. Because of limited time this was excluded from this thesis, and not investigated. It could be interesting to examine the issue of double harmonics to see the responses with this type of loading.

Bibliography

[1] Herbert E. Lindberg. *Little Book of Dynamic Buckling.* LCE Science/Software, Penn Valley, California, 2003.

[2] Jianbei Zhu, Mario M. Attard, and David C. Kellerman. In-plane nonlinear buckling of circular arches including shear deformations. *Archive of Applied Mechanics (Ingenieur Archiv)*, 84:1841–1860, 2014.

[3] Igor A Karnovsky. *Theory of Arched Structures: Strength, Stability, Vibration.* Springer New York, New York, NY, 2012.

[4] Kjell Magne Mathisen. Stress stiffness and buckling analysis, 2017.

[5] Simulia. Abaqus theory guide 6.14, 2014.

[6] Y.-L. Pi, M.A. Bradford, and B. Uy. In-plane stability of arches. *International Journal of Solids and Structures*, 39(1):105–125, 2002.

[7] Thor I Fossen. Parametric resonance in dynamical systems, 2012.

[8] Youqin Huang, Airong Liu, Yonglin Pi, and Wei Gao. Assessment of lateral dynamic instability of columns under an arbitrary periodic axial load owing to parametric resonance. *Journal of Sound and Vibration*, 395:272–293, 2017.

[9] Anthony N. Kounadis and Ioannis G. Raftoyiannis. Dynamic buckling of a 2-dof imperfect system with symmetric imperfections. *International Journal of Non-Linear Mechanics*, 40(10):1229–1237, 2005.

[10] V.V Bolotin. *The dynamic stability of elastic systems.* Holden-Day series in mathematical physics. Holden-Day, San Francisco, Calif, 1964.

[11] Ivar Langen. *Dynamisk analyse av konstruksjoner.* Tapir, Trondheim, 1979.

[12] Wei-Chau Xie. *Dynamic stability of structures.* Cambridge University Press, Cambridge, 2006.

[13] D. E Newland. *An introduction to random vibrations, spectral & wavelet analysis.* Dover, Mineola, N.Y, 3rd ed. edition, 2005.

[14] Arvid Naess. *Stochastic dynamics of marine structures.* Cambridge England, 2013.

[15] Jaap Schijve. *Fatigue of Structures and Materials.* Springer Netherlands, 2nd ed. edition, 2009.

[16] J Singer. *Buckling experiments : experimental methods in buckling of thin-walled structures : Vol. 2 : Shells, built-up structures, composites and additional topics*, volume Vol. 2. Wiley, Chichester, 2002.

[17] Jun Xu and Jie Li. An energetic criterion for dynamic instability of structures under arbitrary excitations. *International Journal of Structural Stability and Dynamics*, 15(2):1–14, 2015.

[18] George Papazafeiropoulos, Miguel Muñiz-Calvente, and Emilio Martínez-Pañeda. Abaqus2matlab: A suitable tool for finite element post-processing. *Advances in Engineering Software*, 105:9–16, March 2017.

[19] Yanyan Sha, Jørgen Amdahl, Aleksander Aalberg, and Zhaolong Yu. Numerical investigations of the dynamic response of a floating bridge under environmental loadings. *Ships and Offshore Structures*, pages 1–14, January 2018.

Appendix A

Cut-off criterion for analysis

As mentioned previously, if the stress in the model reaches yield stress then dynamic buckling is no longer of interest. Hence, this is set as a coarse limit on the analyses in order to scale the output.

For the arch, the analysis provide moment at the midpoint, hence if the moment causes yield stress then the model is considered as having reached the failure point.

For an arch with yield stress $\sigma_y = 355$ N/mm^2 the corresponding moment is

$$M_{max} = \frac{\sigma_y \cdot I}{c} = 5.501 \cdot 10^{11} \text{ Nm}$$

where c is the distance from the neutral axis to the outermost fibre of the cross section, and I is the second moment of area.

Appendix B

MATLAB-script

In this chapter the MATLAB-script used in the analysis can be found.

```
clear all
close all

cd('C:\Users\ingvi\Desktop');

%% get the data from the base input file

fid = fopen('Dynamic_bue.inp','r');
data=textscan(fid,'%s', 'delimiter','\n');
data = data{1};
fclose(fid);

index_start = find(cell2mat(cellfun(@(x) strcmp(x,'*PARAMETER'), data,
'UniformOutput', 0)));
dummy = cellfun(@(x) strfind(x,'**'), data, 'UniformOutput', 0);
dummy = find(cell2mat(cellfun(@(x) ~isempty(x), dummy, 'UniformOutput', 0)));
dummy = dummy(dummy>index_start);
index_end = dummy(1);

% keep parts that wont be modified
cell1 = data(1:index_start);
cell3 = data(index_end:end);


%% parameters of harmonic loading

% frequency vector
fn=0.0103;
f = linspace(fn*0.3,fn*2.5,35);
w = 2.*pi.*f;
% duration
T = 5000;
% amplitude
Pn=35364;
A = linspace(Pn*0.2,Pn*0.4,10);

%%

c = 1;
for i = 1:length(w)

    for j = 1:length(A)
        % modify the input file

        cell2=cellstr(num2str([w(i)], 'omega=%f'));
        cell4=cellstr(num2str([A(j)], 'Load=%.f'));

        % put together
        cell_full = [cell1; cell2; cell4; cell3];

        % print the modified input file
        new_name =
```

```
strcat('Job','_',num2str(T),'_',num2str(w(i)),'_',num2str(A(j)));

        fid = fopen(strcat(new_name,'.inp'),'w');
        fprintf(fid,'%s\n',cell_full{:});
        fclose(fid);

        run_string = ['abaqus job=' new_name];
        dos(run_string)
        pause(10)
        while exist(strcat(new_name,'.lck'),'file')==2
            pause(0.1)
        end
        fprintf(['Analysis ' num2str(c) ' completed\n']);
        c = c+1;
    end

end


%%  post-process the results



u1 = cell(length(w), length(A));
u2 = cell(length(w), length(A));
m2 = cell(length(w), length(A));
time= cell(length(w), length(A));

for i = 1:length(w)

    for j = 1:length(A)

        file_name =
strcat('Job','_',num2str(T),'_',num2str(w(i)),'_',num2str(A(j)),'.fil');
        Rec = Fil2str(file_name);

        % displacements
        out1 = Rec101(Rec);

        indices = find(out1(:,1) == 4); %4 is the node where displacements are
collected from
        u1{i,j} = out1(indices,2);
        u2{i,j} = out1(indices,3);
        nsteps=length(u1{i,j});


               % Moment
        Momentgrense=5.501e11; %Yield criteria
        out2 = Rec13(Rec);
        nintpoints=(length(out2)/nsteps);
        m2{i,j} = out2(1:nintpoints:end,4);
        [~,dummyi] = max(abs(m2{i,j}));
```

```
        m2_max(i,j) = m2{i,j}(dummyi);
            idxmax=find(abs(m2{i,j})>Momentgrense,1);
        if abs(m2_max(i,j))<Momentgrense
            idxmax=numel(m2{i,j});
        else
            idxmax=idxmax(1);
        end


       %Finding max displacement for last part of analysis
        u1{i,j}=u1{i,j}(1:idxmax);    %Finding u1 where M<Momentgrense
        u2{i,j}=u2{i,j}(1:idxmax);
        lhalv=int16(nsteps/1.5); %Last part of the analysis
        if lhalv<idxmax
                [~,dummyi] = max(abs(u1{i,j}(lhalv:end)));
                u1_max(i,j) = u1{i,j}((dummyi+lhalv)-1);
                [~,dummyi] = max(abs(u2{i,j}(lhalv:end)));
                 u2_max(i,j) = u2{i,j}((dummyi+lhalv)-1);
        else
              [~,dummyi] = max(abs(u1{i,j}(idxmax:end)));
              u1_max(i,j) = u1{i,j}(dummyi);
              [~,dummyi] = max(abs(u2{i,j}(idxmax:end)));
              u2_max(i,j) = u2{i,j}(dummyi);

        end

        % Time
        out=Rec2000(Rec);
        time{i,j}=cell2mat(out(:,1));
        timeu2{i,j}=time{i,j}(1:length(u2{i,j}));



    end

end

save('results_parametrix','u1_max','u2_max','m2_max','u1','u2','m2');

%%
load('results_parametrix');
%% Make plots

for freq_ind = 1:length(f)
    for amp_ind = 1:length(A)



        figure;
        plot(time{freq_ind,amp_ind}, m2{freq_ind,amp_ind},'LineWidth',2);
        ylabel('Moment (Nm)');
        xlabel('Time (s)');
```

```
        grid on;
        lstring = ['f = ',num2str(f(freq_ind)), ' Hz', ' P_{max} = ',
num2str(A(amp_ind))];
        legend(lstring);
        set(gca,'FontSize',12);
        saveas(gcf,['moment_series_',num2str(freq_ind),'_',num2str(amp_ind)]);
        close(gcf);
        figure;
        plot(timeu2{freq_ind,amp_ind}, u2{freq_ind,amp_ind},'LineWidth',2);
        ylabel('Displacement (m)');
        xlabel('Time (s)');
        grid on;
        lstring = ['f = ',num2str(f(freq_ind)), ' Hz', ' P_{max} = ',
num2str(A(amp_ind))];
        legend(lstring);
        set(gca,'FontSize',12);
        saveas(gcf,['delta_series_',num2str(freq_ind),'_',num2str(amp_ind)]);
        close(gcf);


    end
end


figure;
abs_m2_max = abs(m2_max);
surf(A,f,abs_m2_max);
ylabel('f (Hz)');
xlabel('P_{max}');
zlabel('Moment_{max} (Nm)');
saveas(gcf,['paxdispmom_',num2str(freq_ind),'_',num2str(amp_ind)]);
close(gcf);


figure;
abs_u2_max = abs(u2_max);
surf((2*A/Pn),(f/fn),abs_u2_max);
ylabel('\omega/\omega_{n}');
xlabel('P_{max}/P_{cr}');
zlabel('\delta (m)');
saveas(gcf,['paxdispsurf_',num2str(freq_ind),'_',num2str(amp_ind)]);
close(gcf);


figure;
abs_u2_max = abs(u2_max);
waterfall((2*A/Pn),(f/fn),abs_u2_max);
ylabel('\omega/\omega_{n}');
xlabel('P_{max}/P_{cr}');
zlabel('\delta (m)');
saveas(gcf,['paxdisp_',num2str(freq_ind),'_',num2str(amp_ind)]);
close(gcf);
```

Appendix C

Challenges with the arch

In this section some of the challenges regarding the analyses with the arch are presented. Initially the arch was modelled with two point masses, each located at a quarter distance from each end. This was done in order to create as simple a system as possible. However, while running analyses with varying frequencies the arch experienced very large deformations for some frequencies, as illustrated in figures C.1 and C.2 below. Attempts were made to remedy this problem; however, the solution proved to be elusive. As a result of this effort, the decision was made to use a distributed mass instead of the two point masses.

In figure C.1 the arch snapped through two times before it became stable, this caused very large deformations, about 500 meters, deformations on this scale will not occur in the real model. Whereas in figure C.2 the arch experienced large deformations, in excess of 300 meters, also an unacceptable result.

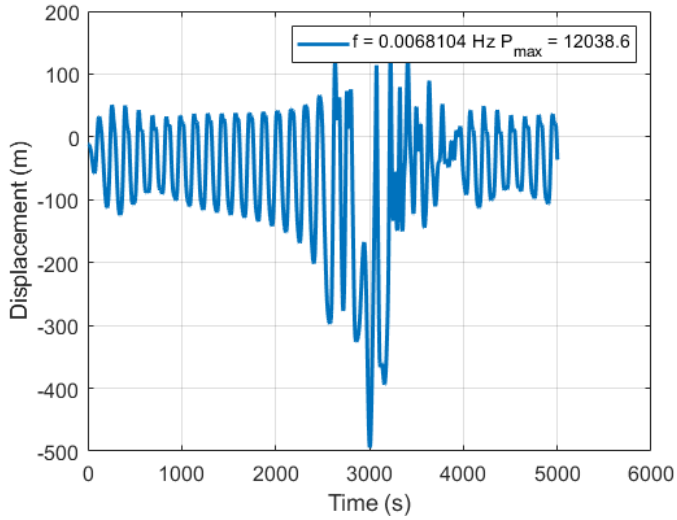

Figure C.1

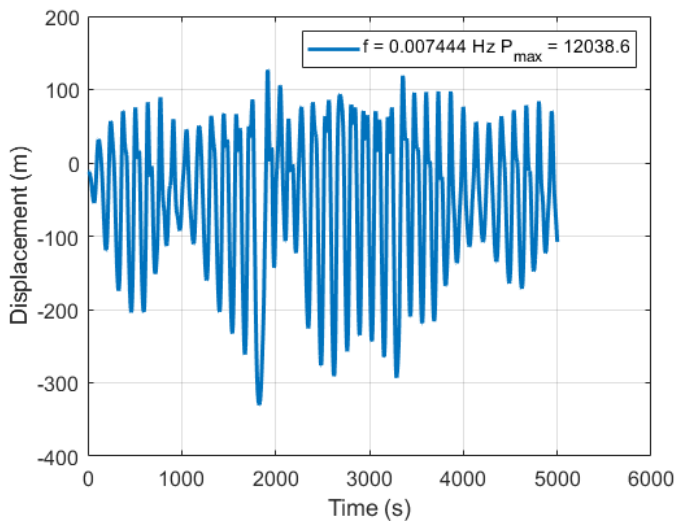

Figure C.2

Appendix D

Stochastic plots

In this section the plots from the stochastic analyses used to determine the stability of the system are presented. Both for the arch and the bridge.

The following plots are from the stochastic analyses of the arch.

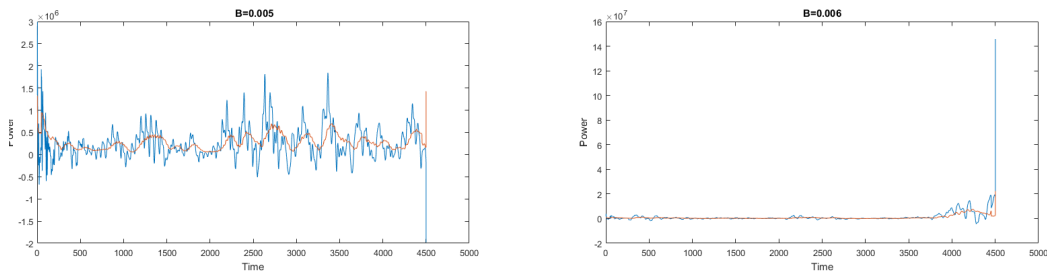

Figure D.1: B = 0.005 and 0.006 respectively

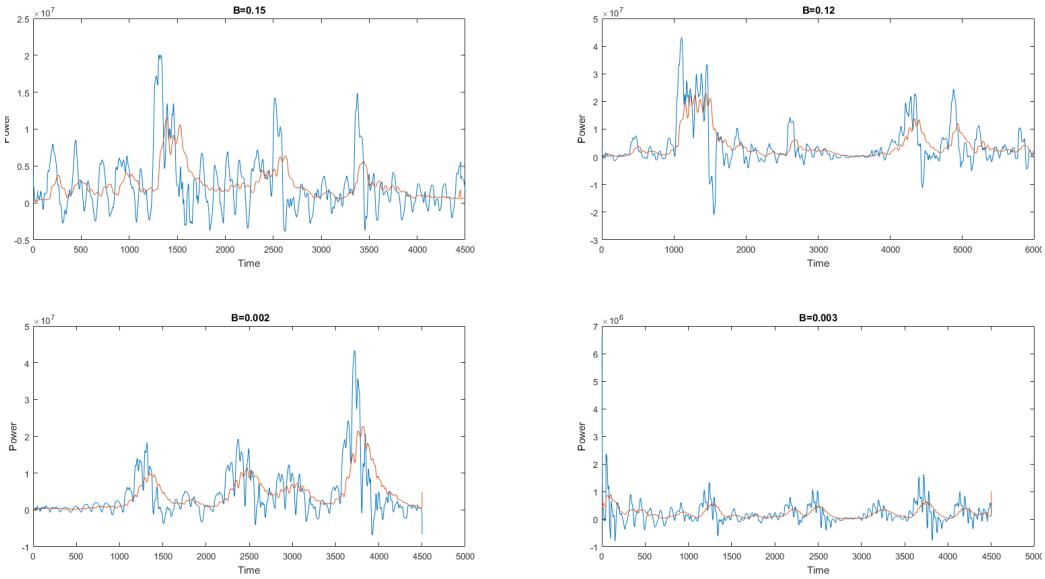

Figure D.2: B = 0.15, B = 0.12, B = 0.002 and B = 0.003

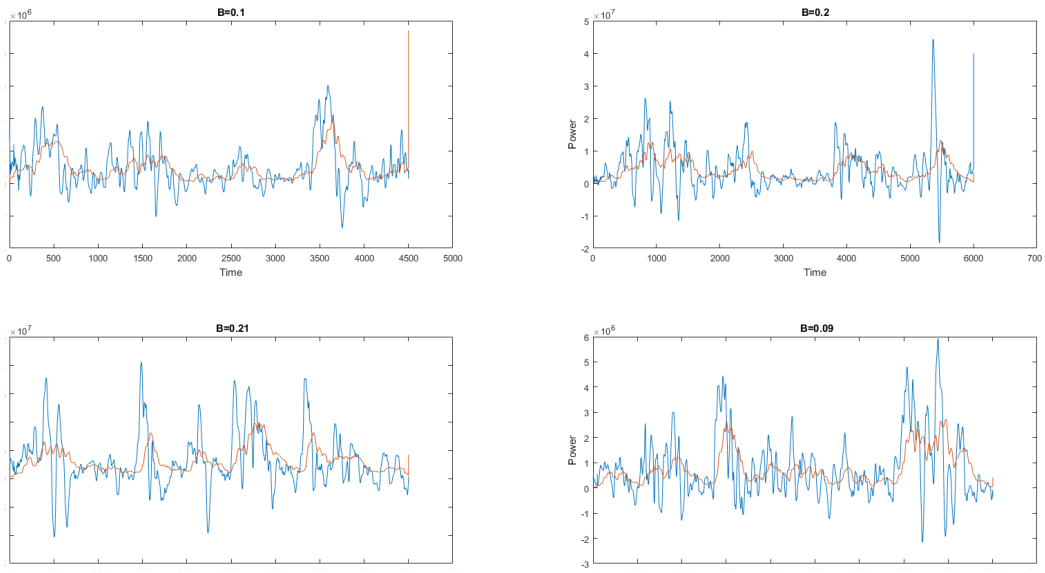

Figure D.3: B = 0.1, B = 0.2, B = 0.21 and B = 0.09

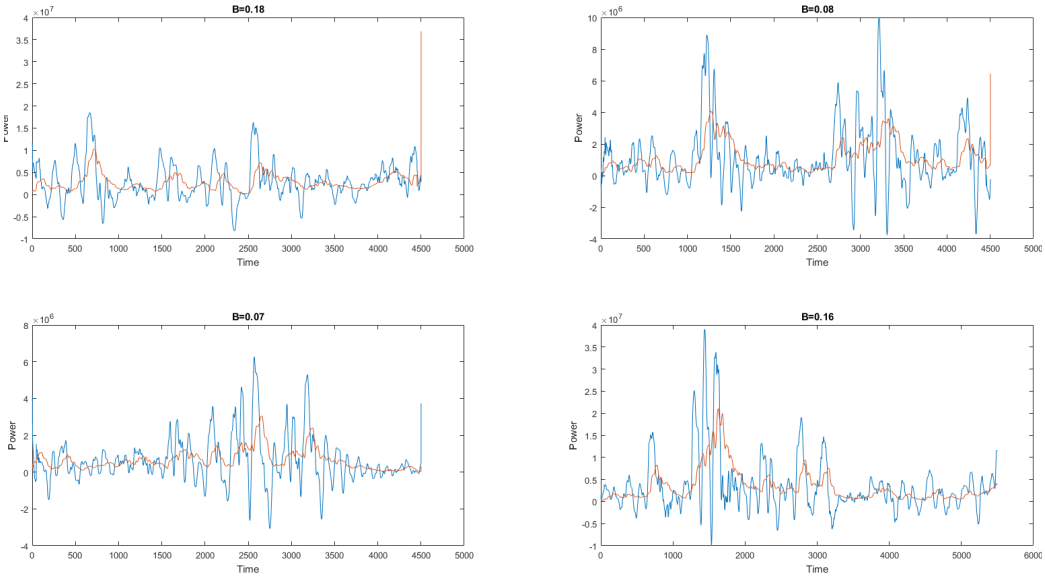

Figure D.4: B = 0.18, B = 0.08, B = 0.07 and B = 0.16

The following plots are from the stochastic analyses of the bridge.

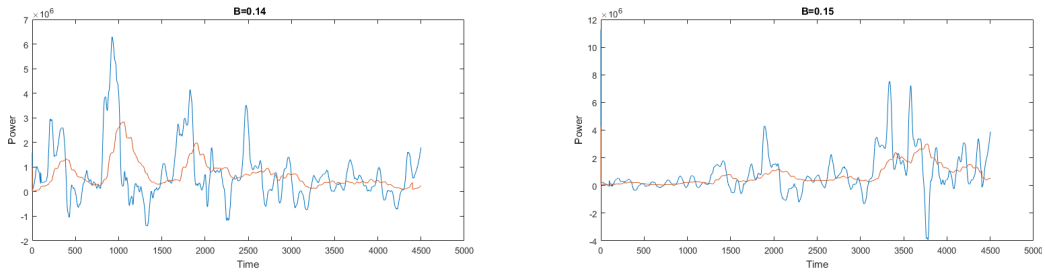

Figure D.5: B = 0.14 and B = 0.15 respectively

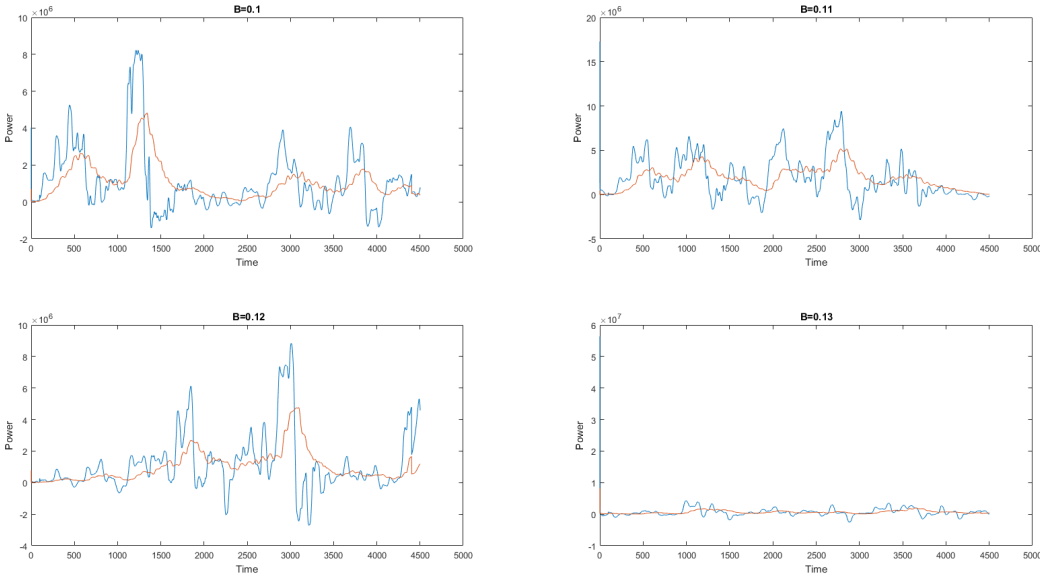

Figure D.6: B = 0.10-0.13 respectively

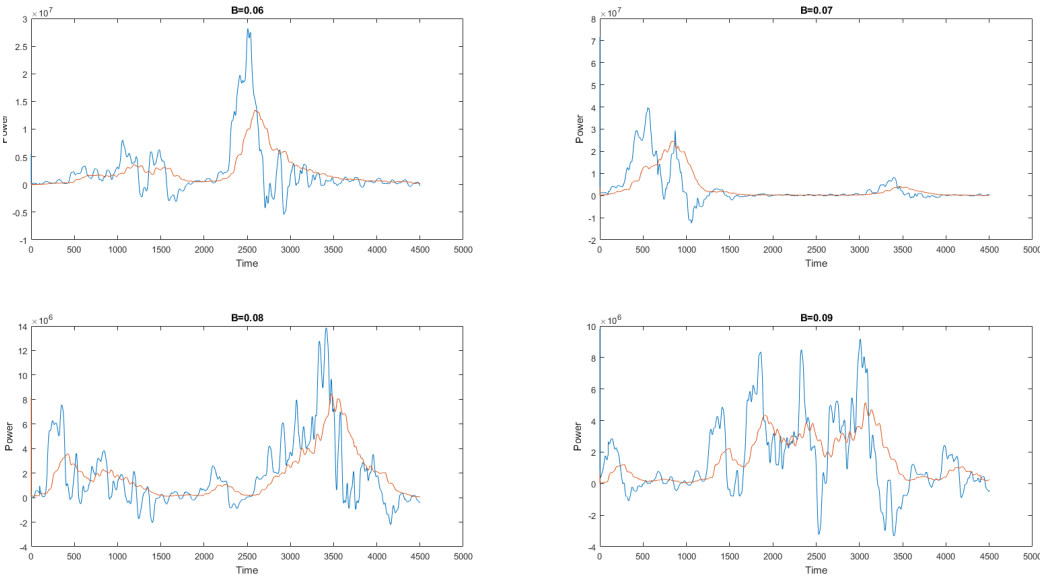

Figure D.7: B = 0.06-0.09 respectively

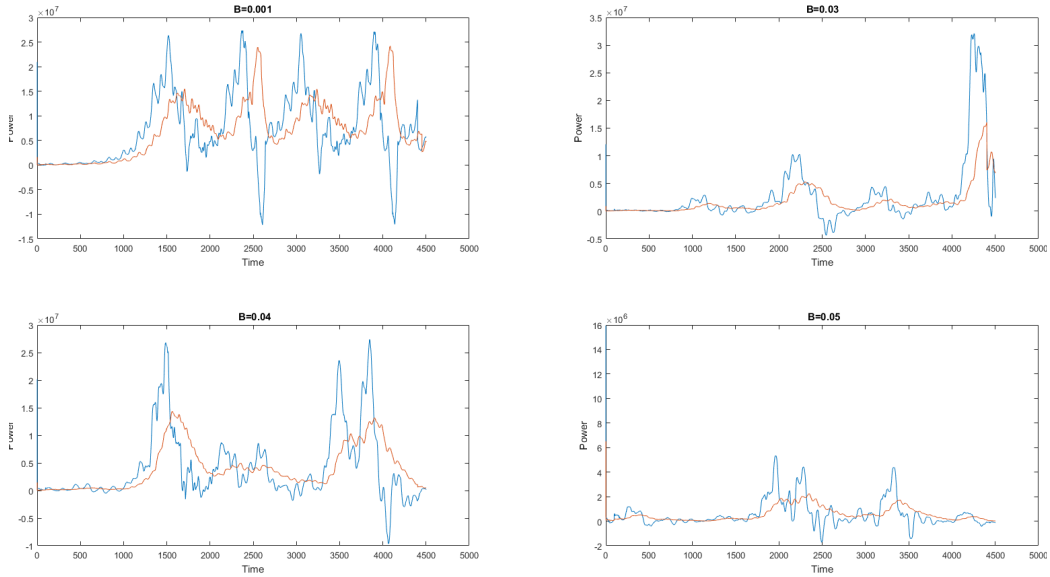

Figure D.8: B = 0.001 and B = 0.03-0.05 respectively